Jujube stones based highly efficient activated carbon for methylene blue adsorption: Kinetics and isotherms modeling, thermodynamics and mechanism study, optimization via response surface methodology and machine learning approaches

Nasma Bouchelkia, Hichem Tahraoui, Abdeltif Amrane, Hayet Belkacemi, Jean-Claude Bollinger, Abdelkrim Bouzaza, Abdelhalim Zoukel, Jie Zhang, Lotfi Mouni

Jujube stones based highly efficient activated carbon for methylene blue adsorption: kinetics and isotherms modeling, thermodynamics and mechanism study, optimization via Response surface methodology and machine learning approaches.

Nasma Bouchelkia[a,b], Hichem Tahraoui[c,d] *, Abdeltif Amrane[e], Hayet Belkacemi[f], Jean-Claude Bollinger[g] , Abdelkrim Bouzaza[h], Abdelhalim Zoukel[i,j], Jie Zhang[k], and Lotfi Mouni[b]

[a] Département de génie des procédés, faculté de technologie, Université de Bejaia, 06000 Bejaia, Algeria. E-mail: nasmabouchelkia@gmail.com. URL : www.univ-bejaia.dz

[b] Laboratory of Management and Valorization of Natural Resources and Quality Assurance, SNVST Faculty, Akli Mohand Oulhadj University, Bouira 10000, Algeria. E-mail: nasmabouchelkia@gmail.com, l.mouni@univ-bouira.dz . URL: www.univ-bouira.dz

[c] Department of Pharmaceutical Engineering, Faculty of Process Engineering, University of Salah Boubnider Constantine 3, Constantine, 25000, Algeria. URL: www.univ-constantine3.dz

[d] Laboratory of Biomaterials and Transport Phenomena (LBMPT), University of MÉDÉA, ALGERIA, Nouveau Pôle Urbain, Médéa University, 26000 Médéa, Algeria. E-mail: tahraoui.hichem@univ-medea.dz , URL: www.univ-Médéa.dz

[e] Univ Rennes, Ecole Nationale Supérieure de Chimie de Rennes, CNRS, ISCR – UMR6226, F-35000 Rennes, France. E-mail: abdeltif.amrane@univ-rennes1.fr, URL: www.univ-Rennes1.fr

[f] Technology Laboratory of Materials and Process Engineering (LTMGP), University of Bejaia, 06000 Bejaia, Algeria. E-mail: belkacemihayet903@gmail.com, URL : www.univ-bejaia.dz

[g] Laboratoire E2Lim, Université de Limoges, 123 Avenue Albert Thomas, 87060 Limoges, France. E-mail: jcbollinger@unilim.fr, URL: www.unilim.fr .

[h] Laboratoire Sciences Chimiques de Rennes – Equipe Chimie et Ingénierie des Procédés, UMR 6226 CNRS, ENSCR, Avenue du Général Leclerc, 35700 Rennes, France ; E-mail: abdelkrim.bouzaza@ensc-rennes.fr , URL: www.univ-Rennes1.fr

[i] Laboratory Physico-Chemistry of Materials, Laghouat University, 03000 Laghouat, Algeria. E-mail: ab.zoukel@lagh-univ.dz, URL : www.lagh-univ.dz

[j] Center for Scientific and Technical Research in Physicochemical Analysis (PTAPC, Laghouat-CRAPC), 03000 Laghouat, Algeria. URL : www.lagh-univ.dz

[k] School of Engineering, Merz Court, Newcastle University, Newcastle upon Tyne NE1 7RU, UK. E-mail: jie.zhang@newcastle.ac.uk, URL: www.ncl.ac.uk

* Corresponding author: Hichem Tahraoui. E-mail: tahraoui.hichem@univ-medea.dz

ABSTRACT

Water contaminated by methylene blue (MB) dye was treated with activated carbon based on locally collected jujube stones. This activated carbon was characterized by physico-chemical methods after preparation and chemical activation. Response surface methodology (RSM) was used to maximize the MB uptake a dependent variable in Box-Behnken Design (BBD) with the initial concentration of methylene blue (400-700 mg/L), adsorbent dosage (0.6-1.6 g/L), contact time (30-540 min), pH (7-11) and temperature (20-50°C) as independent variables. Then, the database created by BBD was further modeled using Gaussian Process Regression coupled with Bagging (Bootstrap Aggregation_Bag) and Dragonfly optimization algorithm (GPR_DA_Bootstrap). The results of the optimization analysis using the GPR_DA_Bootstrap model are shown to be superior to those of the BBD model. The experimental validation of the optimal conditions of the GPR_DA_Bootstrap model (X_1 = 700 mg/L, X_2 = 0.6 g/L, X_3 = 540 min, X_4 = 11, and X_5=50°C) led to an MB uptake (501.01 mg/g) significantly higher than that of BBD (456.00 mg/g). In addition, the very low error between the experimental and the predicted values given by the GPR_DA_Bootstrap model (8.64 mg/g) compared to that of the BBD model (22.19 mg/g), should be highlighted. This clearly shows the efficiency and the performance of the GPR_DA_Bootstrap model on the one hand; as well as the effectiveness of activated carbon prepared from jujube stones (*PJAC*) as a low-cost adsorbent on the other hand.

Graphical abstract

Keywords

Activated carbon; Bootstrap Aggregation_Bag; Box-Behnken design; Dragonfly algorithm; Gaussian Process Regression; Methylene blue adsorption

1. Introduction

Wastewater provided by human activities generates a variety of hazardous substances that degrade and pollute the environment. The discharge of dye-loaded wastewater into the ecosystem affects harmfully the human's health and ecological environment (Abdulhameed et al. 2019). Water characteristics are impacted by the color caused by some dyes which can be visible even at concentrations lower than 1 ppm (Li et al. 2022), and can also provoke toxicity in aquatic environment if they contain metals or some aromatic compounds (Mashkoor and Nasar 2020). Moreover, dyes are not easy to degrade chemically, biologically, and by the light because of their origin and complex structure (Postai et al. 2016; Li et al. 2022). It is therefore crucial to treat them before their evacuation into the ecosystem (Jawad et al. 2020a)

Methylene Blue is a cationic dye widely used in the industrial field to dye wool, cotton and many other fabrics in the textile industry. It is also used as a coloring agent in the paper

industry and in cosmetics for artificial hair dyeing (Pandey et al. 2017). High exposure to methylene blue poses serious health hazards for the environment and humans. It may provoke nausea, vomiting, breathing difficulties, allergy, heart rhythm disturbances, tissue necrosis, skin irritation, mental confusion and even cancer and dysfunction of brain, liver and central nervous system (Pandey et al. 2017; Jawad et al. 2018a). Researchers have, over the years, successfully developed a wide range of techniques for the methylene blue elimination such as electrochemical treatment (Teng et al. 2020), ion exchange (Su et al. 2022), photocatalytic degradation (González-Crisostomo et al. 2022), membrane filtration (Bangari et al. 2022), coagulation-flocculation (Ihaddaden et al. 2022), and Fenton process (Ye et al. 2022). Adsorption, among other techniques, has consistently shown to be one of the most effective and reliable technology for wastewater treatment. It offers the advantages of being simple to use, environmentally friendly and economically efficient with great performance and selectivity (Jawad et al. 2018c; Jawad et al. 2022; Ma et al. 2022). Activated carbon is the most commonly used adsorbent thanks to its characteristics, such as a big specific surface area, presence of diverse surface functional sites, developed porous structure and thermostability, high mechanical strength, as well as its capability of adsorbing huge types of dyes in a wide range of pH (Khoo et al. 2013; Chedri Mammar et al. 2020). The expense of the commercial activated carbon restricted its utilization due to the need for expensive and unsustainable non-renewable raw materials such as coal (Bouchelkia et al. 2016). Hence, low-cost precursors derived from agricultural wastes and characterized by their low organic content and high carbon content are used to prepare an inexpensive efficient activated carbon (Ab Ghani et al. 2017) such as jujube stones (Bouchelkia et al. 2016), banana pseudo-stem (Ab Ghani et al. 2017), apricot stone (Abbas 2021), artichoke leaves (Bencheikh et al. 2021), bamboo (Khuongab et al. 2021), pistachio-nut shell (Cheng et al. 2021), and many others.

In this research, the potential and effectiveness of a non-expensive activated carbon made by chemical activation of locally collected jujube stones using phosphoric acid was tested for the methylene blue (MB) dye sorption. The chemical activation has been chosen because of its advantages over physical activation, including a higher surface area, a comparatively shorter preparation time, and a higher product yield (Jawad et al. 2021). Several experiments have been carried out to examine new efficient chemically activated carbons (Ferreira et al. 2020; Giraldo et al. 2021; Wang et al. 2021; de Souza et al. 2022).

The use of Phosphoric acid (H_3PO_4) as activating agent has been found efficient in activated carbon preparation because it offers the decomposition of the lignocellulosic precursor at relatively low activation temperatures with minimal corrosion to the activation equipment. It also presents itself as a low-cost and environmentally friendly dehydration catalyst allowing the development of microporous and/or mesoporous material with high surface area (Benadjemia et al. 2011; Jawad et al. 2020a; Jawad et al. 2020b). Mbarki et al., (Mbarki et al. 2022) demonstrated that the specific surfaces area of activated carbon prepared with H_3PO_4 were greater than those of ACs generated by activation with $ZnCl_2$ and KOH. Mansouri et al., (Mansouri et al. 2018) have also proved the efficiency of activated carbon prepared by chemical activation with phosphoric acid in comparison with H_2SO_4.

In our previous paper (Bouchelkia et al. 2016), the classical method, named one-factor-at-a-time (OFAT), has been used in the adsorption study. Its principle is based on the optimization of a given parameter, while all the other ones are fixed. The OFAT method is time-consuming and does not consider the interactive aspects between the various factors involved; it supposes that all factors are independent (Mansouri et al. 2018). Such issues could be solved by using statistically designed experiments. Response surface method (RSM) is a combination of statistical and mathematical approaches used for modeling and analyzing different processes in order to depict the main and interaction effects and estimate correlations between

experimental factors and responses. It is a simple and economical optimization method with a few number of experiments, resulting in faster and more effective experiment performance (Asfaram et al. 2016; Mansouri et al. 2018; Alhalili 2022). In the same context, machine learning has also been widely used to solve complex adsorption problems and to provide a better understanding of the adsorption process (Lakshmi et al. 2021). It is a collection of techniques for generating predictive models from databases of training examples (Schneider 2020). The experiential "learning" related to human intelligence is exhibited by machine learning, which has the ability to learn from its analysis by using computational algorithms. These algorithms train the machine to make recommendations or autonomous decisions by using large amounts of data as inputs and outputs to successfully and effectively recognize patterns and essentially "learn." The machine can take an input and predict an output once has been trianed (Helm et al. 2020). Machine learning allows to better understanding of the adsorption phenomena while reducing the workload, needed space, costs, and time required (Lakshmi et al. 2021). Several researchers have performed adsorption modeling and optimization studies by comparing and combining the RSM and machine learning approaches. The main goal of the research study of Onu et al., (Onu et al. 2021) was to apply response surface methodology (RSM), adaptive neurofuzzy inference system (ANFIS), and artificial neural network (ANN) to simulating the uptake of Eriochrome black-T (EBT) dye from aqueous solution using Nteje clay. The EBT dye's adsorption was predicted with great accuracy by the ANFIS, ANN, and RSM models. The results showed that ANFIS was the best predictive model and RSM the least effective for EBT dye adsorption. Ghosh et al., (Ghosh et al. 2015) compared the RSM and the ANN for the simulation and optimization of the biosorption process of Cu(II) by alkali-modified spent tea leaves. The obtained results suggest that RSM had better prediction performance as compared to ANN.

In this study, an experimental approach of RSM, the Box-Behnken Design (BBD), and some machine learning models; Gaussian Process Regression coupled with Bagging (Bootstrap Aggregation_Bag) and Dragonfly optimization algorithm (GPR_DA_Bootstrap), were used to optimize the MB adsorption onto the prepared activated carbon. The models created for the independent variables were optimized for their influence on the dependent variables using the BBD. The initial concentration of methylene blue (400-700 mg/L), the adsorbent dosage (0.6-1.6 g/L), the contact time (30-540 min), the pH (7-11) and the temperature (20-50°C) and response (MB uptake) were taken into account to find the best circumstances. Then, a Gaussian process regression model with Bagging (Bootstrap Aggregation_Bag) and Dragonfly (GPR_DA_Bootstrap) optimization algorithm was used to predict the outputs using the BBD database. After than, optimization by two techniques, dragonfly (DA) and particle swarm (PSO) was caried out to find the optimal for the two models. Finally, an application was created using the MATLAB guide to provide an easy way to implement optimization and prediction of MB uptake. To our knowledge, optimizing the efficiency of activated carbon based on jujube stones used for the treatment of MB from BBD and GPR_DA_Bootstrap has never been attempted before. Moreover, such a comparison has never been made before in this context.

The remaining part of this paper is organised as follows. The method of preparation and activation of activated carbon as well as its characterization are presented in Section 2, where a detailed explanation of the MB uptake isotherms, Kinetics, thermodynamic study and adsorption mechanism are also provided. Furthermore, the experimental design method BBD, the modelling method of GPR_DA_Bootstrap, and the optimization analysis based on two algorithms are also presented in Section 2. Section 3 presents the interpretation of BBD. In addition, the modeling results of GPR_DA_Bootstrap and the optimization results followed by experimental validation are also presented. The last section concludes the paper.

2. Materials and methods

All reactants were of analytical grade and used without additional purification.

2.1. Preparation of the methylene blue stock solution

The methylene blue used (Mw=319.85 $g.mol^{-1}$) is a cationic dye ($C_{16}H_{18}N_3SCl$) purchased from Sigma-Aldrich. Its maximum absorption wavelength is 665 nm (determined by a UV-visible spectrophotometer, Agilent Cary 60). The 2000 mg/L stock solution was prepared by dissolving the adequate amount of MB in 1 L of bidistilled water. It was further diluted to prepare the required concentrations.

2.2. Preparation of activated carbon

The jujube used in this research was picked from Bouira, Algeria. It was harvested between September to December. The stones were first separated from the pulp by heating in boiling water, rinsed with tap water repeatedly, then with distilled water. After that, the stones were dried to constant weight. Crushed stones were sieved and the fraction of 1-2 mm was chemically activated with 85 % phosphoric acid (H_3PO_4) at an impregnation rate of 1/1 by weight. The mixture was refluxed for two hours at the temperature of 200 °C, then carbonized in a furnace (WiseTherm, Witeg Wisd) at 600 °C for one hour. The obtained activated carbon (hereafter named *PJAC*) was finally neutralized with distilled water and dried at 60°C to constant weight, sieved on a 100 µm sieve, and stored in desiccators.

2.3. Characterization of *PJAC*

The approximate analysis of the *PJAC* composition permitted the determination of the ash content (according to ASTM D2866-70), the moisture content (according to ASTM D2867-70), the volatile matter content (according to ISO 562-1981) and the fixed carbon content (according to ASTM D3172) (Bahnes et al. 2018). The true density (ρ_t) was measured by the pycnometer method using methanol as a solvent (Heschel and Klose 1995). The bulk

density (ρ_a) was calculated as described by El Nemr et al.(El Nemr et al. 2021). The porosity ε (%) was then calculated using equation (1) (Heschel and Klose 1995)

$$\varepsilon = \left(1 - \frac{\rho_a}{\rho_t}\right) \times 100 \quad (1)$$

The pore volume (V_p) was determined using the following equation (Tarbaoui et al. 2014)

$$V_P = \frac{1}{\rho_a} - \frac{1}{\rho_t} = \frac{\varepsilon}{\rho_a} \quad (2)$$

The iodine number was determined as described in the standard method AATM 1112-01 (Ahmed and Dhedan 2012).

To determine the methylene blue index and the specific surface area available to methylene blue, it was assumed that its adsorption occurs in a monolayer following the Langmuir equation (Bahnes et al. 2018). A mass of 0.02 g of studied activated carbon was stirred with 20 mL of methylene blue solution at concentrations ranging from 100 to 1000 mg/L, the mixture was stirred for 24 hours at room temperature, then centrifuged and analyzed by UV-visible spectroscopy (Agilent Technologies, Cary 60). The amount of MB adsorbed for each initial dye concentration was determined by the equation (3)

$$q_e = \frac{(C_0 - C_e)}{m} \times V \quad (3)$$

Where, V (L) is the volume of the treated solution, m (g) is the mass of activated carbon used, C_0 (mg/L) represents the concentration of the MB solution at t=0, and C_e (mg/L) is the MB concentration at equilibrium time.

The methylene blue index, represented by q_{max}, was then determined from the Langmuir isotherm. The area available to methylene blue is determined by the following equation (Douara et al. 2016; Bahnes et al. 2018)

$$S_{MB} = \frac{q_{max} N.S}{M} \quad (4)$$

Where S_{MB} ($m^2.g^{-1}$) is the specific surface area, q_{max} is the MB index which represents the maximum adsorption capacity (mg/g) determined from the Langmuir isotherm, N (mol^{-1}) is Avogadro's number ($6.023.10^{23}$ mol^{-1}), S ($Å^2$) represents the surface occupied by a methylene blue molecule (130 $Å^2$) (Hang and Brindley 1970), and M ($g.mol^{-1}$) is the molecular weight of methylene blue (319.85 $g.mol^{-1}$).

The Boehm titration was performed according to the method described in our previous work (Bouchelkia et al. 2016).

The variable pH_{pzc} defines the pH value for which the net charge of the adsorbent surface is zero. First of all, a series of bottles containing 50 mL of 0.1 M NaCl solutions, whose pH was previously adjusted by the addition of 0.1 M NaOH or 0.1 M HCl aqueous solutions to be in the range of 2-10, were prepared. Then, 0.15 g of dried *PJAC* was then added to each bottle. The suspensions were stirred at a speed of 150 rpm for 48 hours at room temperature. Each solution was then filtered and a new pH measurement was performed using a Mettler Toledo pH meter and named pH_{final}. The curve representing $pH_{final} = f(pH_{initial})$ was drawn. The pH_{pzc} corresponds to the pH of the solution for which the curve crosses the first bisector ($pH_{final} = pH_{initial}$) (Bohli et al. 2015; Thangappan et al. 2016).

FTIR analysis was performed on a PerkinElmer Spectrum, to assess the functional groups present on the surface of the raw jujube stone (hereafter named *Raw J*) and *PJAC* before and after adsorption. The activated carbon powder was not pre-treated before being analyzed. The spectra were recorded in the range of 4000 and 400 cm^{-1}.

The X-ray diffraction (XRD) analysis of the samples was performed to investigate their structural features. The X-ray diffraction patterns on powders were collected at room temperature on a Malvern Panalytical X'pert Pro analyzer. The structure analysis of the raw material and the activated carbon was investigated between 2θ angles of 10° - 80° employing a 0.02° step.

To investigate the morphological characteristics of the *Raw J* and *PJAC* before and after adsorption of the MB, the samples were analyzed by Scanning Electron Microscopy (SEM) using Thermoscientific Quattro S Microscope.

N_2 adsorption-desorption technique was used to determine the Surface area and pore distribution of the *Raw J* and *PJAC*. The isotherms were carried out on a Micromeritics ASAP 2020 Plus surface area analyser at 77K which corresponds to the liquid nitrogen temperature. The specific area was estimated using Brunauer–Emmett–Teller (BET) method (Labied et al. 2018)

2.4. Batch adsorption experiments

Adsorption tests were performed by stirring 20 mL of methylene blue of determined concentration with *PJAC* under magnetic stirring at 200 rpm using a multi-stirrer system (Selecta Multimatic-5N). The pH was adjusted using 0.1 M NaOH and 0.1 M HCl solutions. After the adsorption time, the mixture was centrifuged at 3000 rpm for 15 min using a LW Scientific EZ Swing centrifuge, the supernatant was then analyzed spectrophotometrically at a wavelength of 665 nm. Equations 3 and 5 were used to determine the amount of methylene blue adsorbed at equilibrium time, and at any time t onto the *PJAC*, respectively.

$$q_t = \frac{(C_0 - C_t)}{m} \times V \tag{5}$$

Where, V (L) is the volume of the treated solution, m (g) is the mass of activated carbon used, C_0 and C_t, (mg/L) are the MB concentration at t=0 and any time t, respectively. q_t (mg/g) is the amount of adsorbed MB per *PJAC* mass unit at any time t.

2.5. Adsorption kinetics

Studying adsorption kinetics is an important step in elucidating the rate-determining steps, reaction pathways, and dominant mechanisms in the adsorption process (Tan and Hameed 2017; Dao et al. 2021). To determine the kinetics of MB adsorption by *PJAC*, we examined

pseudo-first-order, pseudo-second-order kinetic equations, and intraparticle diffusion models. The corresponding equations are shown in Table 1 (Tran et al. 2017)

2.6. Adsorption isotherms

Adsorption isotherm is the equilibrium relationship between the concentrations of the adsorbed pollutant (solid phase) and its concentration in the solution (liquid phase) at a given temperature (Panadare et al. 2014). The isotherm study provides crucial information on the mechanism of the adsorption process and maximum adsorption capacity (Baidya and Kumar 2021). In this work, Langmuir, Freundlich and Temkin isotherms have been applied to investigate the methylene blue distribution between the liquid and solid phases. Table 1 shows the non-linear forms of the three used models (Tran et al. 2017).

The experimental conditions were pH = 7.0, and the *PJAC* dosage = 1g/L. The initial dye concentration was varied between 100 and 1000mg/L and the temperature of experiments was around 25°C. The agitation rate was fixed to 200rpm.

Table 1: Adsorption kinetics and isotherms models

	Model	**Equation**	**Parameters**
Adsorption kinetics	Pseudo-first-order model	$q_t = q_e(1-e^{-K_1 t})$	K_1 : the pseudo-first-order kinetic rate constant (min^{-1})
	Pseudo-second-order model	$q_t = \frac{q_e^{\,2} K_2 t}{1+q_e k_2 t}$	K_2 : the pseudo-second-order kinetic rate constant ($g \cdot mg^{-1} \cdot min^{-1}$)
	Intraparticle diffusion model	$q_t = K_p t^{1/2} + C$	K_p : intra-particle diffusion rate constant ($mg \cdot g^{-1} \cdot min^{-1/2}$) C a constant related to the boundary layer thickness ($mg \cdot g^{-1}$).
Adsorption isotherms	Langmuir model	$q_e = \frac{q_m K_L C_e}{1+K_L C_e}$	K_L : Langmuir adsorption constant (L/mg) q_{max} : maximum MB

			adsorption capacity (mg/g)
	Freundlich model	$q_e = K_F.Ce^{1/n}$	K_F : Freundlich constant related to adsorption capacity [(mg/g)/(mg/L)^n] n : adsorption intensity constant
	Temkin model	$q_e = (\frac{RT}{b_T}).Ln(K_T.C_e)$	K_T : the equilibrium binding constant representing the maximum binding energy (L/mg). b_T: Timkin constant, a constant related to the heat of adsorption. T: the absolute adsorption temperature (K), R: the gas constant (8.314 J/mol.K).

2.7. Box-Behnken design

The Box-Behnken design (BBD) is a statistical model of response surface methodology (RSM) (Box and Behnken 1960). Empirical and of second-order, it allows the estimation of the parameters of the quadratic model by establishing a relation between the experimental factors and the obtained results (Ferreira et al. 2007; Witek-Krowiak et al. 2014; Sadhukhan et al. 2016). The total number of experiments (N) needed to a BBD is given by the relation: $N = 2K.(K-1)+C_0$ where C_0 represents the number of repetitions of the center point and K is the number of factors (Ferreira et al. 2007). All factors have three coded levels of values, low (-1), medium (0), and high (+1). Non-linear regression was carried out to fit the experimental data with the second-order polynomial given by equation (6) and to determine the relevant model terms:

$$Y = \mathrm{B}_0 + \sum_{i}^{k} \mathrm{B}_i x_i + \sum_{i}^{k} \mathrm{B}_{ii} x^2 + \sum_{ij}^{k} \mathrm{B}_{ij} x_i x_j + E \quad (6)$$

Where Y is the MB uptake (the dependent variable), *k* is the number of independent variables (factors), x_i is the *i*th independent variable in coded level, β_0 is the regression coefficient at the center point. B_i is the linear coefficient for the *i*th independent variable, B_{ii} is the *i*th quadratic coefficients, B_{ij} is the second-order interaction coefficient between the ith and jth independent variables (linear by linear), and E is the error (Das and Das 2014; Shahbazi et al. 2020).

The relation between the actual values and the coded values is described in equation (7)

$$x_i = \frac{X_i - X_0}{\Delta X_i} \quad (7)$$

Where X_i is the actual value of the ith variable; x_i is the coded value of X_i; X_0 is the actual value of X_i at the center point, and ΔX_i is the step change (Han et al. 2013; Moussa et al. 2022).

In this work, the BBD technique, of the RSM approach, was used to optimize the studied process. Regarding the determination of the independent factors, the initial concentration of dye (X_1), the dose of *PJAC* (X_2), the contact time (X_3), the pH (X_4) and the temperature (X_5) were chosen as independent variables; while the MB uptake was chosen as the dependent variable. The JMP program (JMP® Pro 13.0.0) was used to perform the statistical analysis. Interval parameters were determined based on MB uptake as shown in Table 2.

Table 2. Coding and real levels for the BBD model.

Factors	**Coded Levels**		
Independent variables	**-1**	**0**	**+1**
X_1: Initial MB concentration (mg/L)	400	550	700
X_2 : *PJAC* dosage (g/L)	0.6	1.1	1.6
X_3: Contact time (min)	30	285	540
X_4: pH	7	9	11
X_5 : Temperature (°C)	20	35	50

2.8. Gaussian Process Regression coupled with the Dragonfly algorithm

Gaussian Process (GP) is a stochastic process with a series of random variables. Any finite range of those random variables has a joint Gaussian distribution. The probabilistic illustration of a goal function can be used for regression and classification (Tahraoui et al. 2022b; Tahraoui et al. 2022c).

Gaussian Process Regression (GPR) provides a probabilistic, nonparametric strategy for solving nonlinear regression problems. GPR assumes that the measurements of the output variable y are generated in the following way (Park et al. 2017; Liu et al. 2018) :

$$y = f\left(x(k)\right) + \varepsilon \tag{8}$$

where x stands for the measurements of input variables, f is the unknown functional dependence and ε is a Gaussian noise with variance σ_n^2. GPR uses GP as a prior to describe the distribution on the target function $f(x)$ (Park et al. 2017; Tahraoui et al. 2022b). In GPR, the function values $f_{1:n} = (f_1, ..., f_n)$ corresponding to the input $x_{1:n} = (x_1, ..., x_n)$ are treated as random variables, where $f_i = f(x_i)$ (Park et al. 2017; Tahraoui et al. 2022b). GP is defined as a collection of random variables (stochastic process), any finite number of which is assumed to be jointly Gaussian distributed (Park et al. 2017; Tahraoui et al. 2022b). GP can fully describe the distribution over an unknown function $f(x)$ by its mean function $m(x) = E[f(x)]$ and a kernel function $k(x, x')$ that approximates the covariance $E\left[\left(f(x) - m(x)\right)\left(f(x') - m(x')\right)\right]$. The kernel (covariance) function represents a geometrical distance measure assuming that the more closely located inputs would be more correlated in terms of their function values (Park et al. 2017; Tahraoui et al. 2022b). That is, the prior on the function values is represented as (Park et al. 2017; Tahraoui et al. 2022b):

$$\left(f^{1:n}\right) = GP\left(m(\cdot), k(\cdot,\cdot)\right) \quad (9)$$

where:

$m(.)$ = a mean function capturing the overall trend in the target function value, and $k(.,.)$ = a kernel function used to approximate the covariance.

In GPR, the kernel (covariance) function describes the structure of the target function. Thus, the type of kernel function $k(x, x')$ used to build a GPR model and its parameters can strongly affect the overall representability of the GPR model and affect the accuracy of the prediction model. A wide variety of kernel functions can be used (Williams 2005).

In this article, the uptake of MB was also predicted using a GPR model developed from the experimental data under BBD. In order to obtain a better model and better performance, the database was normalized from the beginning in the interval [-1.1], and then it was divided into two sets: 75% for learning and 25% for validation. Then, ten Kernel functions were optimized (exponential, exponential squared, matern32, matern52, quadratic rational, exponential ard, exponential squared ard, ardmatern32, ardmatern52, and quadratic rational ard) with the basis function (constant, linear and zero). The functions of the ten used kernel were given in the supplementary materials section (equations S1 to S10). The knowledge of each Kernel function was also optimized for their specific parameters (Kernel Scale [sigmaM, sigmaF] and sigma) (see Figure 1). For this, the dragonfly algorithm was used to optimize the specific parameters of each Kernel function, since this optimization algorithm has been used to solve a wide variety of optimization problems including solving different machine learning optimization problems (Moussa et al. 2022). Numerous studies have proved that machine learning performance has been improved when the hyper-parameters were optimized using the Dragonfly algorithm (Moussa et al. 2022).

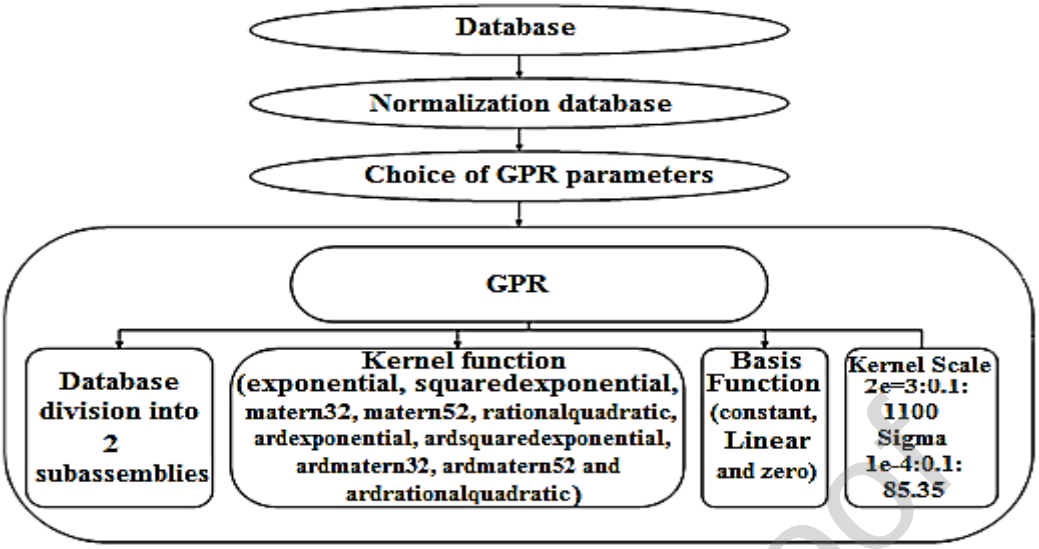

Figure 1. Organization chart for the development and optimization of the GPR_DA model

2.9. Statistical evaluation criteria

Statistic analysis and ANOVA were used to investigate the statistical abilities of the model generated with a confidence level of 95%. The statistical adequacy of the model was assessed using a variety of variables, including the P-value, the value F, the coefficient of variance (C.V), the coefficient of determination (R^2), the adjusted determination of the coefficient (R_{adj}^2), and the Root Mean Square Error (RMSE) for BBD model (Tahraoui et al. 2021b; Tahraoui et al. 2022a; Tahraoui et al. 2022b). The value F describes the variation of the responses, which can be checked by a regression equation, while the value P determines the statistical adequacy of the developed model. For a model to be significant, the P-value must be less than 5%, and the P-value for the inadequacy test must be greater than 5% (Kıvanç and Yönten 2020; Singh and Kumar 2020).

On the other hand, the Correlation Coefficient (R), R^2, R_{adj}^2, and RMSE, were used to evaluate the performance of each GPR_DA model. These are calculated using the equations S11-S13 (supplementary materials) (Belsley et al. 2005; Hong et al. 2007; Tahraoui et al.

2020; Bousselma et al. 2021; Tahraoui et al. 2021a; Tahraoui et al. 2021b; Tahraoui et al. 2022a; Tahraoui et al. 2022b; Tahraoui et al. 2022c).

3. Results and discussion

3.1. Characterization studies

In this work, activated carbon was prepared by chemical activation of Jujube stones (*Ziziphus lotus L*) using 85 % phosphoric acid at a carbonization temperature of 600 °C. The prepared *PJAC* was characterized by FTIR for the study of its chemical structure and the functional groups present on its surface. Actually, the surface of the activated carbon does not only contain carbon atoms, but also other hetero-elements such as sulfur and nitrogen, etc. linked to the carbon atoms, which form the chemical composition of the surface of the activated carbon (Prahas et al. 2008).

Figure 2 reports the N_2 adsorption-desorption isotherms for the *Raw J* and the *PJAC*. Figure 2a shows a type II isotherm according to the IUPAC classification (Peñafiel et al. 2021). This type of isotherm characterizes non-porous or high pore diameter materials (Jawad et al. 2022). Table 3 shows that the *Raw J* is characterized by a specific surface area of 2.0788 m^2/g, which confirms its non-porous character. The rapid rise in adsorption that exhibits the *Raw J* at high pressure (P/Po > 0.95) suggests the retention of macropores (Jawad et al. 2022). On the other hand, the *PJAC* isotherm was found to be similar to Type I isotherm according to the IUPAC classification (Figure 2b), indicating that the *PJAC* is microporous and the adsorption process involves the primary filling of microspores at low relative pressure P/P_0 (Selmi et al. 2018; Daoud et al. 2019). The isotherm also showed that no horizontal plateau was clearly reached, indicating pore enlargement (Selmi et al. 2018). The formation of hysteresis loops indicates the existence of mesopores (Mbarki et al. 2022). As can be seen in Table 3, the specific surface area of the *PJAC* was 685m^2/g with a total volume in pore of

0.425 cm²/g, while the *Raw J* was characterized by a specific surface area of 2.0788 m²/g and a total volume in pore of 0.00192 cm²/g.

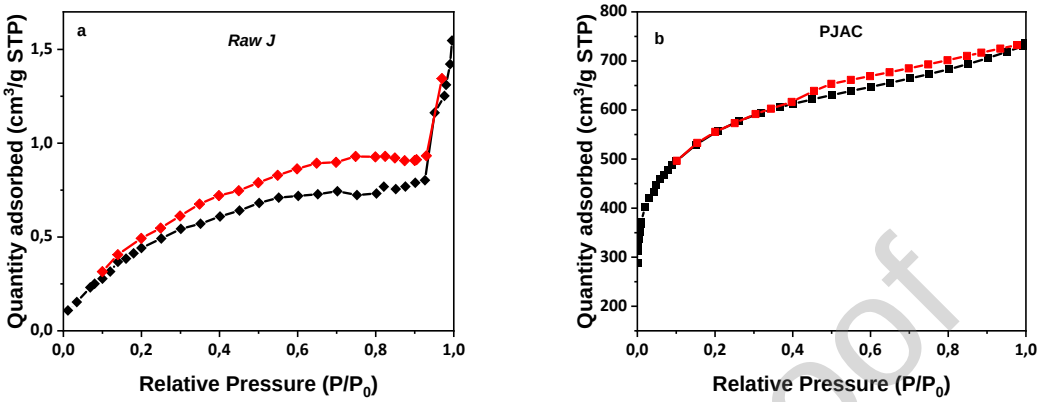

Figure 2. N_2 adsorption-desorption isotherms for (a) *Raw J*, and (b) *PJAC*

Table 3: Textural properties of *Raw J* and *PJAC* materials.

	Raw J	***PJAC***
BET Surface area (m²/g)	2.079	685.000
Langmuir surface area (m²/g)	5.937	1 055.630
Micropore surface area (m²/g)	/	268.638
External surface area (m²/g)	3.289	416.362
Total Volume in Pores (cm²/g)	0.002	0.425

The scanning electron microscopy (SEM) is used as a valuable tool for examining the morphology, the porosity development and the surface structure of the *Raw J*, *PJAC* and *MB-PJAC*. Fig.3 shows the obtained SEM images for the three samples. The surface of the *Raw J* is presented in Figure 3(a), which shows a compact, irregular surface with no discernible pore structure. Figure 3(b) shows a porous and irregular rough structure of *PJAC* in comparison with *Raw J* due to the chemical activation with phosphoric acid and carbonization leading to the release of volatile maters such as lignin and some other organic compounds and to the formation of the porous structure of the activated carbon (Labied et al. 2018; de Souza et al. 2022). The porosity of *PJAC* facilitates the adsorption of BM as shown in Figure 3(c) in

which the surface seems more charged and the pores are less remarkable due to the deposition of MB dye molecules all over the surface.

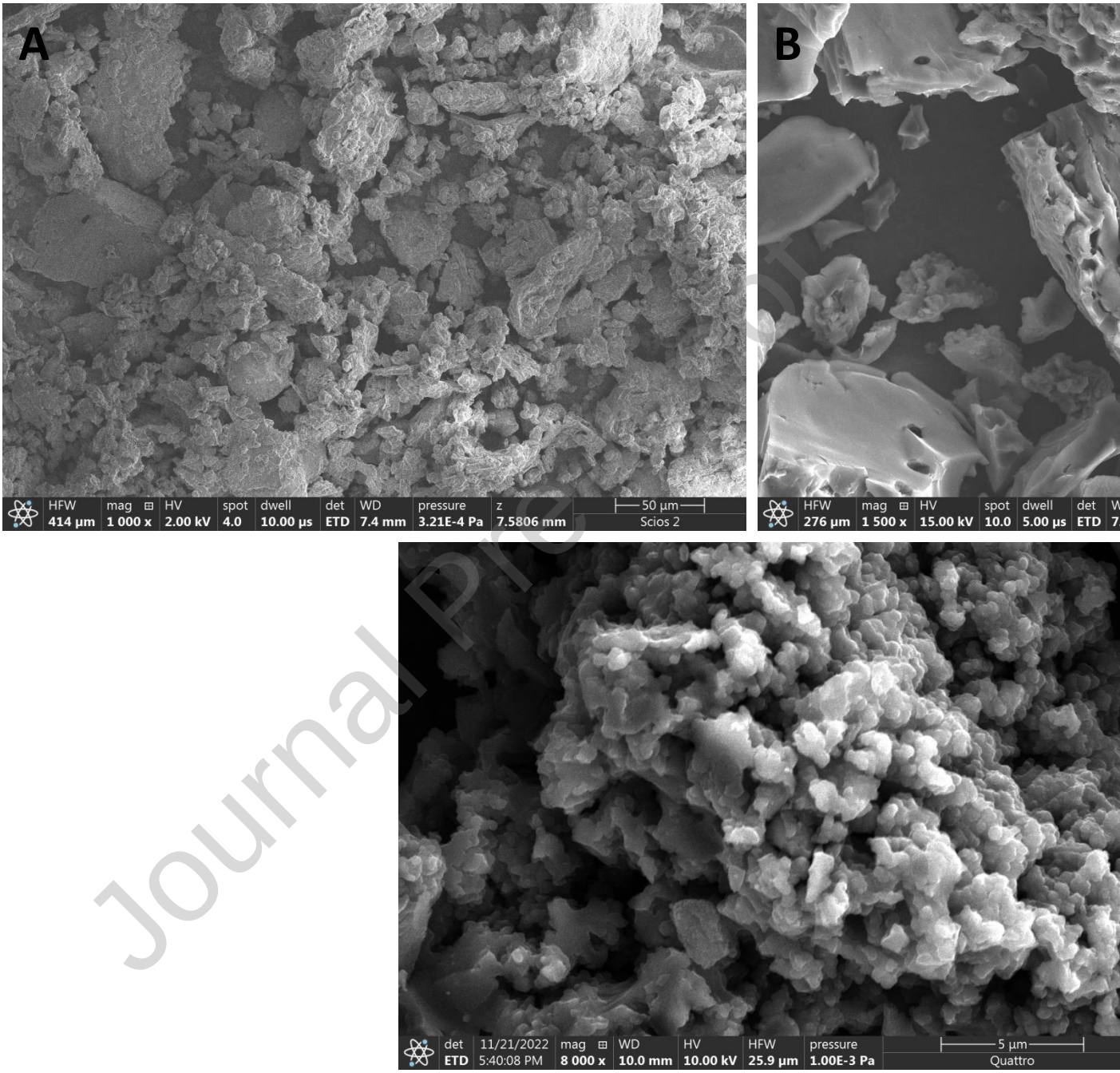

Figure 3. SEM micrographs of samples (A) *Raw J*, (B) *PJAC* and (C) *MB-PJAC*

The FTIR spectrum of raw jujube stone (*Raw J*), and *PJAC* before and after methylene blue adsorption (MB-*PJAC*) are shown in Figure 4.

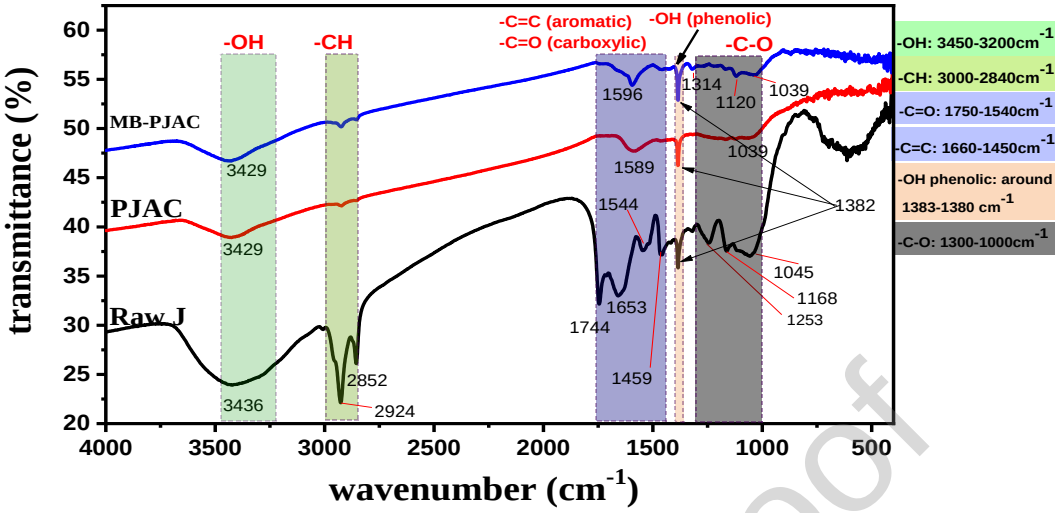

Figure 4. FTIR spectrogram of samples *Raw J*, *PJAC* and *MB-PJAC*

FTIR spectrum of the *Raw J* is shown in Figure 4. The band at 3436 cm^{-1} corresponds to the stretching vibrations of the -OH groups (hydroxyl groups) (Daoud et al. 2019; Shahrokhi-Shahraki et al. 2021). The peaks at 2924 and 2852 cm^{-1} may be assigned to the C-H stretching vibration in the saturated aliphatic groups (alkyl/alkane). The presence of the band at around 1740cm^{-1} can be ascribed to the C=O stretching in aldehyde, ketone esters and acetyl (Shamsuddin et al. 2016; Li et al. 2020; Shahrokhi-Shahraki et al. 2021). The peak at 1653cm^{-1} is attributed to the vibration of C=C in aromatic rings (Boudechiche et al. 2019). The weak peaks at 1544 and 1459 cm^{-1} may be attributed to the existence of C=H bending and C=C cycle stretching mode of aromatic rings (Daoud et al. 2019; Shahrokhi-Shahraki et al. 2021; Teong et al. 2021). Band at around 1382 cm^{-1} correspond to phenolic O-H bending in the *Raw J* (Üner et al. 2016). Peaks at 1253, 1168, and 1045 cm^{-1} indicate the existence of stretching vibrations band of C-O and/or C–O–C in phenols, acids, alcohols, ester, and/or ethers groups (Jawad et al. 2018c; Jawad et al. 2019).

FTIR spectrum of the *PJAC* is also shown in Figure 4. It can be noticed that the intensity of the peak at around 3400 cm^{-1} decreased in comparison with the *Raw J*. The graphs also show that the peaks at around 2900 and 2800 cm^{-1} almost disappeared. This diminution

indicates that phosphoric acid (H_3PO_4) acted as a dehydrating agent; it also removed a significant amount of hydrogen from the *Raw J (*Kundu et al. 2015). The band at 1740 cm^{-1} disappeared, due to the complete removal of ketones and aldehydes groups that are thermally unstable (Shamsuddin et al. 2016), and also to the breaking of many bonds in aliphatic and aromatics species. The comparison shows an almost complete disappearance of some peaks in the *PJAC*, at 1653, 1544, 1459, and 1168 cm^{-1}, and some peaks were slightly shifted to low wavenumber due to the effect of carbonization and chemical activation (Daoud et al. 2019). The activation at high temperature degraded some functional groups that were originally present in the raw material structure (Li et al. 2020). The spectra also showed the appearance of a new peak in the *PJAC* at 1589 cm^{-1}, indicating the C=O stretching vibration of carbonyl and lactone groups (Hesas et al. 2013).

The spectra of prepared activated carbon before and after MB adsorption are shown in Figure 4. Both spectra showed a few changes in the frequencies and intensities of some bands after methylene blue adsorption. The peak at around 1382 cm^{-1}, was almost unchanged, but its intensity was enhanced (Chen et al. 2011) which suggests the involvement of O-H band in the adsorption. Some peaks were slightly shifted indicating their involvement in the adsorption mechanism (Guarín-Romero et al. 2019; Jawad and Surip 2022). For example, the peak at 1589cm^{-1} had shifted of 7cm^{-1}, suggesting the involvement of carboxylic and aromatics (C=O, C=C) groups in the MB uptake. The spectra also showed the appearance of a new peaks in the MB-*PJAC* at 1120 and 1315 cm^{-1}, attributed to C–O and/or C-O-C stretching vibration and to N–H bending, respectively (Chen et al. 2011; Aravind et al. 2022), which reflects the involvement of the C-O, C-O-C and N-H bands in the adsorption mechanism.

The characteristics of the raw jujube stones (*Raw J*) and the prepared activated carbon *PJAC* are summarized in Table 4. The pH_{pzc} of the prepared activated carbon was found to be 5.00, indicating that the surface of *PJAC* is acidic. The surface charge becomes net negative

above pH_{pzc} and MB adsorption is enhanced at higher solution pH (Thangappan et al. 2016). The H_3PO_4 treatment of the *Raw J* led to the diminution of the pH_{pzc} of the produced *PJAC*.

The analysis of the global characteristics of the raw material (Table 4) showed that it had a high amount of volatile matter (75.25 %) and a low amount of ash (0.86 %), which are desired for the production of adsorbents (Rozada et al. 2005). The carbonization and activation processes lead to the release of volatile matter as gas and liquid; the produced activated carbon is then characterized by a low volatile matter content and high fixed carbon content (Msaada et al. 2018). As shown in Table 4, the volatile matter in the *PJAC* decreased from 75.25 % to 45.06 % compared with the raw material. Fixed carbon indicates char carbon (Bahnes et al. 2018); and the results showed that chemical activation induced an increase in carbon content, this is due to the release of volatiles, leading to the elimination of non-carbon content and the enrichment of carbon (Daoud et al. 2019). Similar results have been reported in previous work (Daoud et al. 2019). Ash content is a measurement of non-combustible substances and the non-volatile components of the material (Angın 2013) and good activated carbon must be characterized by a low ash content (Kibami et al. 2014). Accordingly, the prepared *PJAC* was found to have 1.03 % of ash content.

Bulk density, porosity, iodine, and methylene blue adsorption and Surface area are some of the parameters usually examined while evaluating the performance and the porosity structure of produced activated carbons. Table 5 shows the obtained results. Bulk or apparent density defines the weight of material contained in a given volume. This volume includes not only the skeletal solid's volume, but also the pores of the particles and the voids between them (Yeganeh et al. 2006). The prepared *PJAC* was found to have a bulk density of 0.84 g/cm^3 and a porosity of 71.33 %.

Table 4. Characteristics of *Raw J* and *PJAC*

Parameter	*Raw J*	*PJAC*

particles size (µm)	<100 µm	<100 µm
pH_{pzc}	6.60	5.00
Moisture content (%)	7.66	6.50
Ash content (%)	0.86	1.03
Volatile matter (%)	75.25	45.06
Fixed carbon (%)	16.23	47.41

The iodine number is the number of milligrams of iodine absorbed by one gram of activated carbon under specified conditions. A high iodine value indicates a good activation of the adsorbent used and proves its reliability in the removal of small-size pollutants (microporous) (Du et al. 2021). The *PJAC* was characterized by a high iodine number; 867.54 mg/g which confirmed a good development of the microporous surface. The methylene blue index is another fundamental parameter for the characterization of the efficiency and activity of an adsorbent. It is defined as the quantity of MB (in milligrams) adsorbed by one gram of carbon (Bahnes et al. 2018). The methylene blue index found for *PJAC* was 387.61 mg/g. The MB index of *PJAC* is higher than the 299 mg/g obtained via chemical activation of the jujube stone by KOH (700 °C activation temperature for a 3 hours carbonization time), by Bahnes et al. (Bahnes et al. 2018), and the value of 364.2 mg/g obtained by Abdulhameed et al. (Abdulhameed et al. 2021), via chemical activation of biomass of grass waste using a K_2CO_3-assisted pyrolysis approach. The Boehm titration is employed as a chemical approach for identifying oxygen surface groups on carbon compounds. It is built on the concept that different acidities of oxygen groups on carbon surfaces can be neutralized by varying strengths of bases (Bouchelkia et al. 2016) . For the *PJAC*, the number of basic groups was measured as 0.15 $mmol.g^{-1}$, while those of acidic groups were 0.25, 0.51, and 0.60 $mmol.g^{-1}$ for lactonic, phenolic and carboxylic groups, respectively. The total acidic amount on the

PJAC surface was therefore 1.36 mmol.g^{-1}, indicating the predominance of acidic functional groups on the *PJAC* surface.

Table 5. Porosity structures of the *PJAC*

parameter	value
True density (g/cm^3)	2.93
Bulk density (g/cm^3)	0.84
porosity (%)	71.33
Pore volume (g/cm^3)	0.85
Iodine number (mg/g)	867.54
Methylene blue index (mg/g)	387.61
S_{MB} (m²/g)	948.84
Carboxylic groups (mmol/g)	0.60
Lactonic groups (mmol/g)	0.25
Phenolic groups (mmol/g)	0.51
Total acid (mmol/g)	1.36
Total basic (mmol/g)	0.15

X-ray diffraction patterns of the *Raw J* and *PJAC* are given in Figure 5. No significant sharp peaks were observed, which indicated that the *Raw J* and the activated carbon are amorphous materials (Tang et al. 2021). The *Raw J* pattern showed one broad and intense peak at around 21.5°, indicating typical amorphous carbon (Wu et al. 2016). The peak disappeared when the *Raw J* was activated with H_3PO_4 and carbonized at 600 °C and two broad diffraction peaks at 2θ=25° and 43° appeared, corresponding to the reflection of (0 0 2) and (1 0 0) planes, indicating the presence of dehydrated hemicelluloses (Liou 2010; Rezma et al. 2019). At the same time, there are noise signals related to the carbon powder, indicating a predominantly amorphous structure of *PJAC* (Bouchelkia et al. 2016).

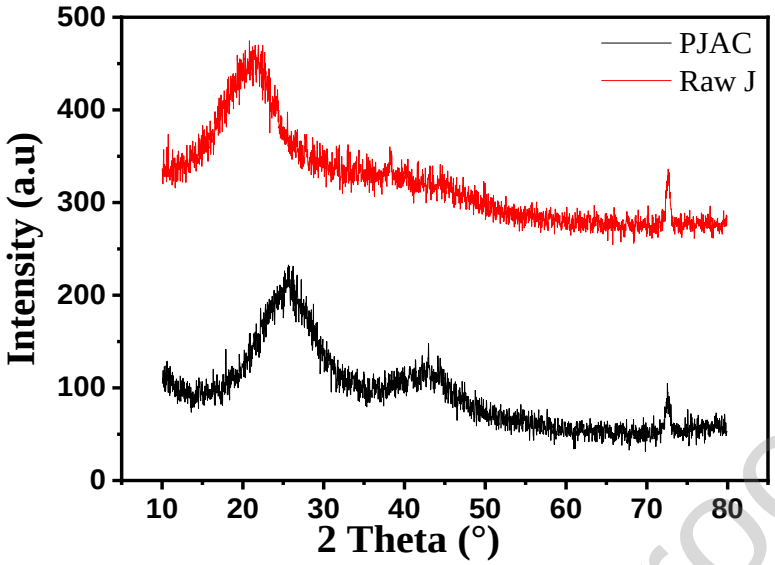

Figure 5. X-ray diffraction pattern of the *Raw J* and *PJAC*

3.2. Adsorption kinetics

In this study, three of the most commonly used kinetic models were applied to investigate the kinetic data of the MB adsorption on the *PJAC* adsorbent, including pseudo-first-order, pseudo-second-order kinetic equations, and intraparticle diffusion model.

The fitting of the kinetic models to the experimental data is represented in Figure 6, and the calculated kinetic parameters are shown in table 6. As can be observed in Table 6, the pseudo-second-order model gave the highest correlation coefficient (R^2> 0.99) compared to the pseudo-first order model, and the calculated q_{ecal} values from this model were also in good agreement with experimental values. Similarly, from the RMSE values, it could also be concluded that the pseudo-second-order kinetic model was better than the pseudo-first-order kinetic model in fitting the adsorption of MB by *PJAC*. A similar conclusion had been reported by Mouni et al. (Mouni et al. 2018) and Dao et al. (Dao et al. 2021).

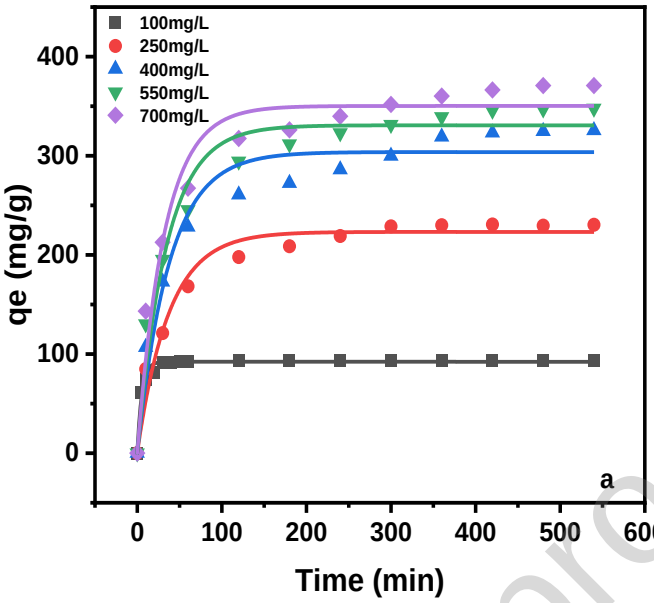

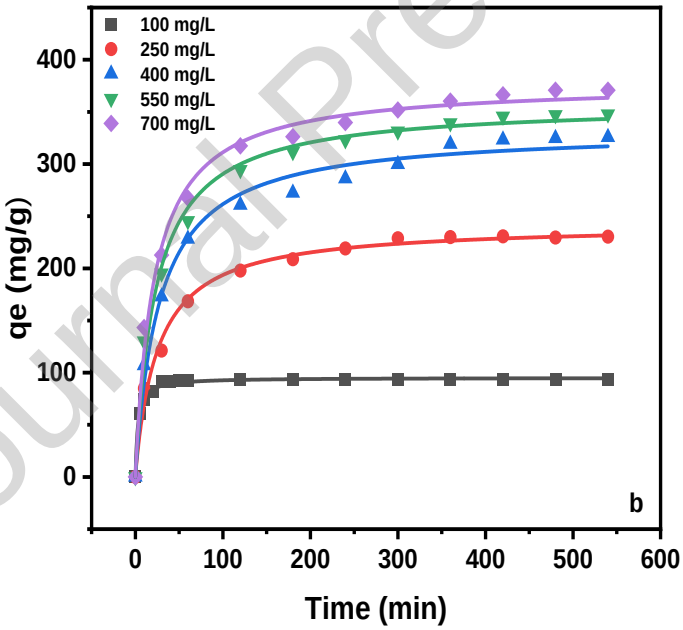

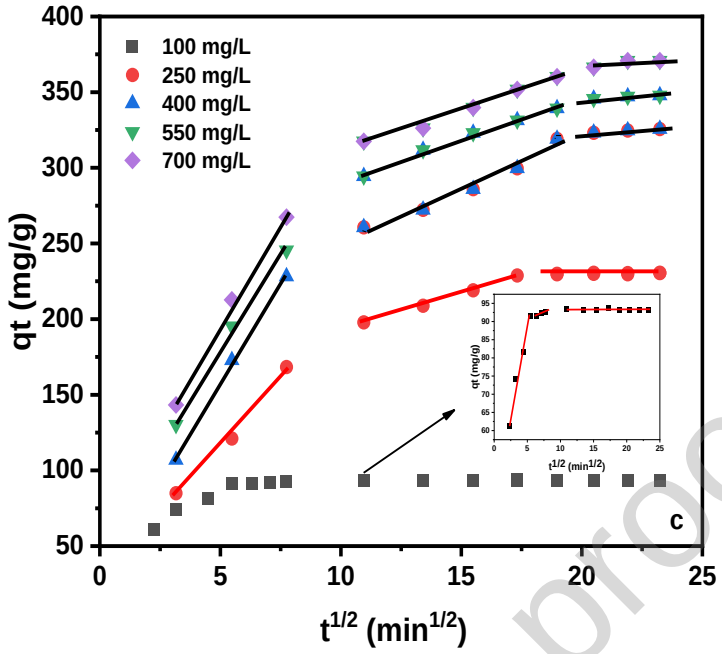

Figure 6. Adsorption kinetic models (a) pseudo-first-order kinetic model, (b) pseudo-second-order kinetic model, (c) intraparticle diffusion model. (Adsorbent dosage=1.00 g/L, Time=540min, T=25°C and pH=7, agitation rate=200 rpm)

Table 6. Adsorption kinetic parameters of MB dye adsorption onto *PJAC* (Adsorbent dosage=1.00 g/L, Time=540min, T=25°C and pH=7, agitation rate=200 rpm)

	Pseudo-first order kinetic					**Pseudo-second order kinetic**			
C_0 ($mg.L^{-1}$)	**qe_{exp} ($mg.g^{-1}$)**	**qe_{cal} ($mg.g^{-1}$)**	**K_1 (min^{-1})**	**R^2**	**RMSE**	**qe_{cal} ($mg.g^{-1}$)**	**K_2 ($g{\cdot}mg^{-1}{\cdot}min^{-1}$)**	**R^2**	**RMSE**
100	**93.268**	**92.184**	**0.188**	**0.985**	**2.841**	**95.029**	**0.004**	**0.994**	**1.736**
250	**230.198**	**223.171**	**0.027**	**0.967**	**12.886**	**242.326**	**$1.639.10^{-4}$**	**0.991**	**6.331**
400	**324.457**	**303.746**	**0.026**	**0.951**	**21.619**	**332.948**	**$1.098.\ 10^{-4}$**	**0.987**	**10.789**
550	**347.426**	**330.715**	**0.029**	**0.959**	**20.975**	**357.956**	**$1.201.\ 10^{-4}$**	**0.993**	**8.937**
700	**370.751**	**350.227**	**0.031**	**0.956**	**22.777**	**377.838**	**$1.235.\ 10^{-4}$**	**0.992**	**9.999**
	Intraparticle diffusion model								

	First stage			Second stage			Third stage		
C_0 (mg/L)	K_{P1} ($mg.g^{-1}.min^{-1/2}$)	C_1 ($mg.g^{-1}$)	R^2	K_{P2} ($mg.g^{-1}.min^{-1/2}$)	C_2 ($mg.g^{-1}$)	R^2	K_{P3} ($mg.g^{-1}.min^{-1/2}$)	C_3 ($mg.g^{-1}$)	R^2
100	**8.811**	**43.314**	**0.972**	**0.828**	**86.368**	**0.994**	**0.019**	**92.774**	**0.925**
250	**25.276**	**18.209**	**0.993**	**4.870**	**143.977**	**0.998**	**0.256**	**224.730**	**0.982**
400	**26.462**	**14.593**	**0.999**	**7.142**	**178.711**	**0.971**	**0.895**	**304.880**	**0.985**
550	**25.165**	**52.869**	**0.995**	**5.526**	**235.793**	**0.991**	**0.779**	**329.780**	**0.972**
700	**27.090**	**59.760**	**0.996**	**5.541**	**254.684**	**0.988**	**1.607**	**334.148**	**0.771**

The application of the intraparticle diffusion model (Figure 6) showed three linear segments implying the involvement of three stages during the MB adsorption process; (1) surface or film diffusion, (2) pore or intraparticle diffusion, and (3) sorption on the interior sites of the adsorbent (Teong et al. 2021). In the first step, the dye diffused quickly through the liquid film to the external activated carbon surface. This step is characterized by the highest values of intraparticle diffusion rate constant (K_p) and the lowest value of the constant C (Table 6). In the second stage, the MB molecules diffused into the internal pores of the *PJAC*. The third stage represents the final equilibrium step where the low residual MB concentration left in the solution moved slowly from larger pores to micropores. It is characterized by the lowest value of K_p and the highest value of C which provides information about the boundary layer thickness, i.e. higher C value implies greater the effect of the boundary layer, reducing then the diffusion of the dye modules due to the occupation of the majority of the adsorption sites (Han et al. 2020). The intraparticle diffusion is considered as the rate determining step when the fitted linear relationship plot passed through the origin (El Nemr et al. 2021). However, in

this study, the fitted lines do not pass through the origin, which proves that intraparticle diffusion is involved but not the only rate-limiting step.

3.3. Adsorption isotherms

Langmuir, Freundlich and Temkin adsorption isotherms are plotted in Figure 7 and the computational parameters are listed in Table 7. The results indicate that the Langmuir model (R^2=0.984, RMSE=3.134) fits the experimental data better than the Freundlich and Temkin isotherms (R^2=0.811, RMSE=6.114 and R^2=0.896, RMSE=5.305 respectively) suggesting that the Langmuir isotherm could be more suitable to describe the behavior of MB adsorption on the prepared *PJAC*. The Langmuir model supposes that adsorption process is monolayer and occurs on a homogeneous surface and that there is no interaction between the adsorbed molecules (Aminu et al. 2020). The value of the Langmuir parameter K_L is between 0 and 1, indicating that the *PJAC* tends to adsorb MB (Ren et al. 2021). The essential characteristics of a Langmuir isotherm can be expressed in terms of a constant (dimensionless) separation factor, R_L that is used to predict whether an adsorption system is "favorable" or "unfavorable". The separation factor R_L is defined by the following equation (Weber and Chakravorti 1974)

$$R_L = \frac{1}{1 + K_L.C_0} \tag{10}$$

Where C_0 (mg/L) is the maximum initial concentration of dye. The isotherm is unfavorable when R_L>1 and it is favorable when 0 < R_L<1. The calculated value of R_L was found to be 0.016 indicating the favorability of the adsorption process. Similarly, the adsorption capacity constant n of the Freundlich isotherm is 5.051 confirming the favorability of the process (Baidya and Kumar 2021).

Table 7. Isotherm parameters for MB adsorption onto *PJAC* (Adsorbent dosage=1.00g/L, Time=540min, T=25°C and pH=7, agitation rate=200 rpm)

Isotherm Model	Parameters values
Langmuir	q_{max}= 387.606 mg/g
	K_L= 0.062 L/mg
	R^2=0.984
	RMSE=3.134
Temkin	K_T=1.442 L/mg
	b_T= 41.068
	R^2=0.896
	RMSE=5.305
Freundlich	K_F= 115.370 [(mg/g)/(mg/L)^n]
	1/n=0.198
	R^2=0.811
	RMSE=6.114

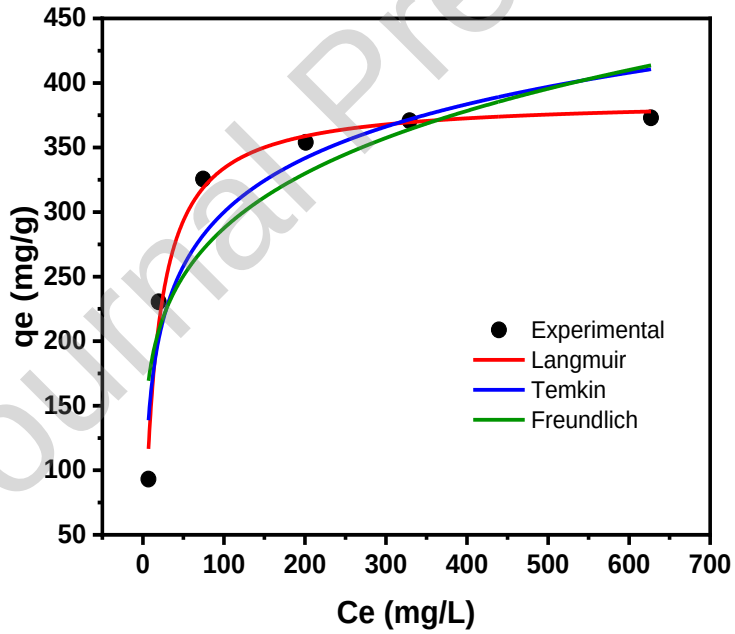

Figure 7. Isotherm models for MB adsorption onto *PJAC* (Adsorbent dosage=1.00 g/L, Time=540min, T=25°C and pH=7, agitation rate=200 rpm).

3.4. The BBD analysis

The optimization of Methylene blue adsorption on the *PJAC* was performed by the BBD approach. The effect of Initial MB concentration (500-700 mg/L), *PJAC* dosage (0.6-1.6 g/L),

Contact time (30-540 min), pH (7-11), and temperature (20-50 °C) were studied using the Box Behnken design. The statistical analysis of the data was performed using JMP program (version 13 pro). Table 8 reports the experimental runs for examining MB adsorption on *PJAC*, as well as the experimental results and predicted values. The number of experiments was set to 46.

Table 8. MB uptake with experimental and predicted value according to BBD

RUN	Initial MB concentration (mg/L)	*PJAC* dosage (g/L)	Contact time (min)	pH	Temperature (°C)	MB uptake (mg/g), experiment values	MB uptake (mg/g), predicted values
1	550	1.1	285	7	20	225.82 ± 4.79	236.66
2	550	1.1	30	9	20	202.55 ± 1.44	201.07
3	550	0.6	285	9	20	321.43 ± 5.77	328.02
4	400	1.1	285	9	20	260.09 ± 5.26	243.40
5	700	1.1	285	9	20	299.26 ± 7.67	299.73
6	550	1.6	285	9	20	198.65 ± 4.56	205.60
7	550	1.1	540	9	20	302.26 ± 9.97	303.23

8	550	1.1	285	11	20	295.40 ± 3.96	287.75
9	550	1.1	30	7	35	210.53 ± 4.10	222.41
10	550	0.6	285	7	35	339.01 ± 6.05	329.50
11	400	1.1	285	7	35	277.40 ± 6.40	280.45
12	700	1.1	285	7	35	313.92 ± 5.21	317.61
13	550	1.6	285	7	35	270.97 ± 2.69	259.05
14	550	1.1	540	7	35	340.87 ± 8.12	336.86
15	550	0.6	30	9	35	312.37 ± 3.62	302.04
16	400	1.1	30	9	35	231.02 ± 2.02	231.18
17	700	1.1	30	9	35	325.22 ± 3.22	307.01
18	550	1.6	30	9	35	224.25 ± 3.97	226.64
19	400	0.6	285	9	35	336.60 ± 5.48	342.09
20	700	0.6	285	9	35	380.65 ± 5.27	386.72
21	400	1.6	285	9	35	280.80 ± 3.52	275.62
22	700	1.6	285	9	35	318.71 ± 5.02	314.12
23	550	0.6	540	9	35	388.91 ± 7.16	387.94
24	400	1.1	540	9	35	352.94 ± 8.31	357.21
25	700	1.1	540	9	35	378.62 ± 7.80	364.51
26	550	1.6	540	9	35	312.51 ± 9.60	324.26
27	550	1.1	30	11	35	285.96 ± 2.25	297.07
28	550	0.6	285	11	35	382.73 ± 5.40	380.59
29	400	1.1	285	11	35	313.11 ± 3.86	328.05
30	700	1.1	285	11	35	358.45 ± 4.45	374.02
31	550	1.6	285	11	35	316.52 ± 2.56	311.97
32	550	1.1	540	11	35	370.99 ± 8.36	366.18

33	550	1.1	285	7	50	336.61 ± 4.16	332.62
34	550	1.1	30	9	50	303.85 ± 1.46	308.34
35	550	0.6	285	9	50	367.22 ± 4.14	372.01
36	400	1.1	285	9	50	361.07 ± 2.34	355.03
37	700	1.1	285	9	50	370.73 ± 4.83	381.84
38	550	1.6	285	9	50	350.20 ± 5.01	355.35
39	550	1.1	540	9	50	382.76 ± 9.17	389.71
40	550	1.1	285	11	50	408.01 ± 5.17	385.54
41	550	1.1	285	9	35	328.31 ± 1.45	331.21
42	550	1.1	285	9	35	333.77 ± 1.28	331.21
43	550	1.1	285	9	35	327.25 ± 1.98	331.21
44	550	1.1	285	9	35	342.53 ± 5.66	331.21
45	550	1.1	285	9	35	331.37 ± 0.08	331.21
46	550	1.1	285	9	35	324.04 ± 3.59	331.21

Table 9 reports the regression analysis (ANOVA) response surface quadratic model for the methylene blue adsorption. Results showed an F-value of 41.611, a P-value of < 0.0001, a coefficient of variance C.V. of 3.742 %, a lack of fit of 0.067 and an R^2 of 0.971, namely very close de the value of the R^2_{adj} (0.948). This confirmed the high significance of the model and the accuracy and the reliability of the experiments.

The suitability of the model can be judged by plotting the predicted values versus the actual values (Zhong et al. 2016). The relationship between the measured and predicted values is shown in Figure 8. It can be seen that the obtained values are distributed very close to the straight line with a high R^2 (0.971), which confirms the relevance of the model and its good prediction of the MB adsorption on *PJAC.*

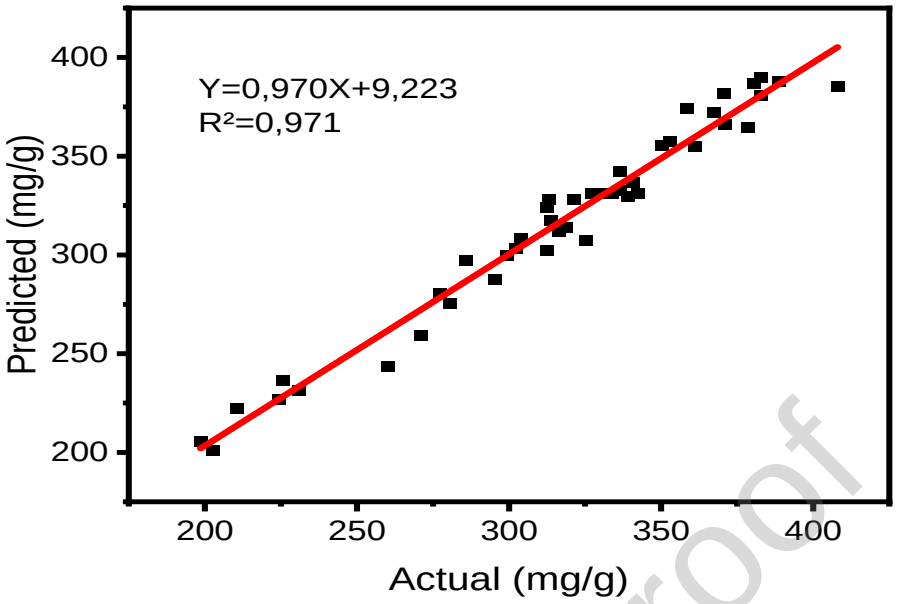

Figure 8. Plot of the predicted vs. actual values for MB uptake on the *PJAC*

Table 9. ANOVA of the BBD for the optimization of the elimination of the MB onto *PJAC*

Source	Degree of freedom	Sum of squares	Mean Squares	F-value	P-value Prob.>F
Model	20	117319.310	5865.970	41.611	<0.0001
Linear					
x_1	1	6911.013	6911.013	49.024	<0.0001
x_2	1	19342.551	19342.551	137.210	<0.0001
x_3	1	33682.343	33682.343	238.931	<0.0001
x_4	1	10818.080	10818.080	76.740	<0.0001
x_5	1	37538.094	37538.094	266.283	<0.0001
Quadratic					
$x_1 * x_1$	1	22.058	22.058	0.157	0.6958
$x_2 * x_2$	1	87.435	87.435	0.620	0.4384
$x_3 * x_3$	1	2772.987	2772.987	19.671	0.0002
$x_4 * x_4$	1	526.580	526.580	3.735	0.0647

x_5* x_5	1	1429.923	1429.923	10.143	0.0039
Interaction					
x_1* x_2	1	9.425	9.425	0.067	0.7981
x_1* x_3	1	1173.748	1173.748	8.326	0.0079
x_2* x_3	1	34.340	34.340	0.247	0.6259
x_1* x_4	1	19.448	0.138	0.138	0.7134
x_2* x_4	1	0.837	0.837	0.006	0.9392
x_3* x_4	1	513.249	513.249	3.641	0.0679
x_1* x_5	1	217.710	217.710	1.544	0.2255
x_2* x_5	1	2796.294	2796.294	19.836	0.0002
x_3* x_5	1	108.160	108.160	0.767	0.3894
x_4* x_5	1	0.828	0.828	0.006	0.9395
Residual	25	3524.270	140.970		
Total	45	120843.580			
Lack of fit	20	3314.051	165.703	3.941	0.0671 [a]
Pure error	5	210.222	42.044		

Regression results	**R^2**	0.971	**R^2_{adj}**	0.948
	RMSE	11.873	**C.V (%)**	3.742

RMSE: Root Mean Square Error. **C.V.**: Coefficient of variance. **lack of fit**[a] : non-significant (> 0.05)

Where the second-order polynomial model can be written as follows:

$$\text{MB uptake } (\text{mg/g}) = \begin{aligned} &331.21 + 20.78\times x_1 - 34.76\times x_2 + 45.88\times x_3 \\ &+ 26.00\times x_4 + 48.43\times x_5 - 17.82\times x_3\times x_3 - \\ &12.80\times x_5\times x_5 - 17.13\times x_1\times x_3 + 26.44\times x_2\times \\ &x_5 + 1.58\times x_1\times x_1 - 3.16\times x_2\times x_2 - 7.76\times x_4\times \\ &x_4 - 1.53\times x_1\times x_2 + 2.93\times x_2\times x_3 + 2.20\times x_1\times \\ &x_4 + 0.45\times x_2\times x_4 - 11.32\times x_3\times x_4 - 7.37\times x_1\times \\ &x_5 - 5.2\times x_3\times x_5 + 0.45\times x_4\times x_5 \end{aligned} \quad (11)$$

Independent variables with high explanatory power for the dependent variable were taken; the five independent variables significantly affected the MB uptake (P-value < 0.0001). The quadratic contact time (x_3^2) and quadratic temperature (x_5^2) terms had also significant effects on the adsorption. The methylene blue elimination by the *PJAC* was also significantly affected by some interaction terms; x_1*x_3 (initial BM concentration and contact time) and x_2*x_5 (*PJAC* dosage et temperature). Contrarily, all other terms were insignificant (P-value > 0.05). So the relationship could be reduced to equation 12:

$$\text{MB uptake } (\text{mg/g}) = 331.21 + 20.78\times x_1 - 34.76\times x_2 + 45.88\times x_3 + 26.00\times x_4 + 48.43\times x_5 - 17.82\times x_3\times x_3 - 12.80\times x_5\times x_5 - 17.13\times x_1\times x_3 + 26.44\times x_2\times x_5 \quad (12)$$

The value of the coefficient of determination decreased slightly (R^2 = 0.957), the equation became simpler after removing the low explanatory power variables from the dependent variable.

3.4.1. Response surface analysis

The Box Behnken design was used to study the effect of the operating parameters (contact time, pH, Temperature, *PJAC* dosage and initial dye dosage) on the adsorption of methylene blue on activated carbon. The response surface analysis is a relevant way to determine the effects and interactions between the 5 selected parameters. The individual effects and the interactions of process variables are discussed below.

3.4.1.1. Effect of contact time

The contact time between adsorbent and adsorbate can be used to determine the potential initiation of binding and the optimum time for contaminant confiscation adsorption. Furthermore, it is a crucial factor governing the kinetics of the adsorption process and overseeing the use of an adsorbent for industrial application and influencing its cost-effectiveness (Mashkoor and Nasar 2020).

Figures 9b, 9c, 10b and 11a show the 3D simulation diagrams of the combined effects of contact time with initial MB concentration, temperature, *PJAC* dosage, and pH, respectively. In each combination, all other parameters were set to their respective mean values. It can be seen from the surface response plots that MB adsorption initially progressed at a high rate due to the availability and accessibility of vacant surface sites. Adsorption sites become inaccessible and the remaining vacant surface sites are difficult to occupy due to the repulsive forces between the molecules of BM on the surface of the solid (adsorbed) and those of the aqueous phase (free) (Bouchelkia et al. 2016). In addition, the molecules have to pass deeper and farther through the pores, which slow down the adsorption rate. Finally, the adsorption process reaches equilibrium.

3.4.1.2. Effect of the initial dye concentration

The MB adsorption was carried out at initial dye concentrations ranging from 400 to 700 mg/L. The 3D simulation diagrams of the combined effects of initial BM concentration and *PJAC* dosage, contact time, pH and temperature are represented in Figures 9a, 9b, 9d and 10a, respectively. In each combination, all other parameters were set to their respective mean values. It can be depicted from the plots that the variation of the initial dye concentration from 400 to 700 mg/L induced an increase of the adsorbed quantity whatever the value of the other factors. This can be explained by the increase of the driving forces between the two phases; liquid and solid, i.e. an increase in the concentration gradient in the medium (Mehmood et al. 2015). Same results have been reported by Baidya and Kumar. (Baidya and Kumar 2021).

Table 5 shows that the interaction between contact time and initial MB concentration was significant with a p-value of 0.0079. The plot represented in Figure 9b was obtained for an initial MB concentration range of 400 to 700 mg/L and varying contact time from 30 to 540 min at a fixed temperature, pH, and *PJAC* dosage of 35°C, 9 and 1.1 g/L (middle values), respectively. As discussed above, the dye uptake increased with the adsorbent contact time until the equilibrium; and at a given time, the removal of methylene blue increased with the increase of MB initial concentration.

3.4.1.3. Effect of pH

Figures 9d, 10c, 11a and 11b show the 3D simulation diagrams of the combined effects of pH with initial MB concentration. *PJAC* dosage, contact time, and temperature, respectively. In each combination, all other parameters were set to their respective mean values. It can be noticed from the response surface plots that MB uptake increased with the increase of pH from 7 to 11. As previously mentioned, the pH_{pzc} of the *PJAC* was 5.00. When the solution pH is lower than the pH_{pzc}, the net surface charge is positive, which favors the adsorption of anions. On the other hand, solution pH higher than the pH_{pzc} favors the adsorption of cations; and the net surface charge becomes more negatively charged while increasing the pH (Jawad et al. 2018b). This explains the enhancement in the elimination of methylene blue with the increase of the pH of the solution. A similar trend was found by Dotto et al. (Dotto et al. 2015) in the adsorption of MB onto Ultrasonic Surface Modified Chitin.

3.4.1.4. Effect of *PJAC* dosage and temperature

Table 9 shows that the interaction between *PJAC* dosage and temperature was the most significant as compared to all the other interactions with a p-value of 0.0002. Figure 10d shows the 3D simulation diagrams of the combined effects of *PJAC* dosage and temperature. Experiments were carried out within the *PJAC* dosage range (0.6 – 1.6 g/L) and temperature range (20 - 50 °C) at a fixed initial MB concentration, contact time and pH of 550 mg/L, 285

min and 9 (middle values), respectively. The response surface plot shows that, at a fixed temperature, MB uptake decreased with the increase in *PJAC* dosage due to the decrease in adsorbate to adsorbent ratio (Baidya and Kumar 2021). The plot also shows that the MB uptake increased while increasing the temperature from 20 to 50°C. A similar trend was observed in the response surface diagrams shown in Figures 9c, 10a, and 11b where the increase in temperature increased the dye elimination, which indicates that the MB is favorably adsorbed by *PJAC* at high temperatures. This could be explained by the increase in the mobility and diffusion of the methylene blue molecules due to the reduction of the viscosity of the solution (Li et al. 2020). The temperature rise may also increase the porosity of the *PJAC* pore and improves the accessibility of active sites. The increase of the BM uptake by increasing the temperature suggests that the adsorption may be an endothermic process (Baidya and Kumar 2021). This can be explained by the calculation of thermodynamic parameters based on the Van't Hoff equation. These parameters were developed assuming that the adsorbate is uniformly distributed on the surface of the adsorbent. The adsorption thermodynamic parameters, such as Gibbs free energy change (ΔG^0, kJ/mol), enthalpy change (ΔH^0, kJ/mol) and entropy change (ΔS^0, kJ/mol.K), were determined according to following equations: (Huang et al. 2019; Han et al. 2020; Jawad et al. 2022)

$$\ln K_d = \frac{\Delta S^\circ}{R} - \frac{\Delta H^\circ}{RT} \tag{13}$$

$$K_d = \frac{q_e}{C_e} \tag{14}$$

$$\Delta G^\circ = -RT.Ln(K) \tag{15}$$

$$\Delta G^\circ = \Delta H^\circ - T\Delta S^\circ \tag{16}$$

Where K_d is the equilibrium constant, qe is the amount of MB adsorbed at equilibrium (mg/L), Ce is the concentration of MB remaining in the solution at equilibrium (mg/L), T is

the absolute adsorption temperature (K), and R is the gas constant (8.314 J/mol.K). The plot of ln(K_d) vs. 1/T (figure not shown) was used to determine the values of ΔH^0 and ΔS^0 from the slope and the intercept of the Van't Hoff equation 13, respectively. ΔG^0 was calculated at different temperatures using equation 16 (Gao et al. 2020) The obtained results are shown in Table 10. The reported results show that the ΔG^0 is negative revealing that the adsorption process was spontaneous in nature and occurred automatically (Ren et al. 2021). The negative value of ΔG^0 decreased with increasing adsorption temperature, indicating that the adsorption process was stimulated at high temperature (Gao et al. 2020). The enthalpy change ΔH^0 confirms that the process was endothermic (Huang et al. 2019). The ΔH^0 value is less than 40 kJ/mol, indicating that the adsorption of MB on the *PJAC* is mainly of physical nature (Peñafiel et al. 2021). ΔS^0 was also positive which reflect the random disorder nature of the interface between the solid and the liquid during the MB adsorption process (Gao et al. 2020; Jawad et al. 2022).

Table 10. Thermodynamic parameters of the MB adsorption on the *PJAC*

Adsorbent	T (K)	ΔG° (kJ/mol)	ΔH° (kJ/mol)	ΔS° (kJ/mol.K)	R^2
PJAC	293	-0,687	21,414	0,075	0,998
	303	-1,442			
	313	-2,196			
	323	-2,950			

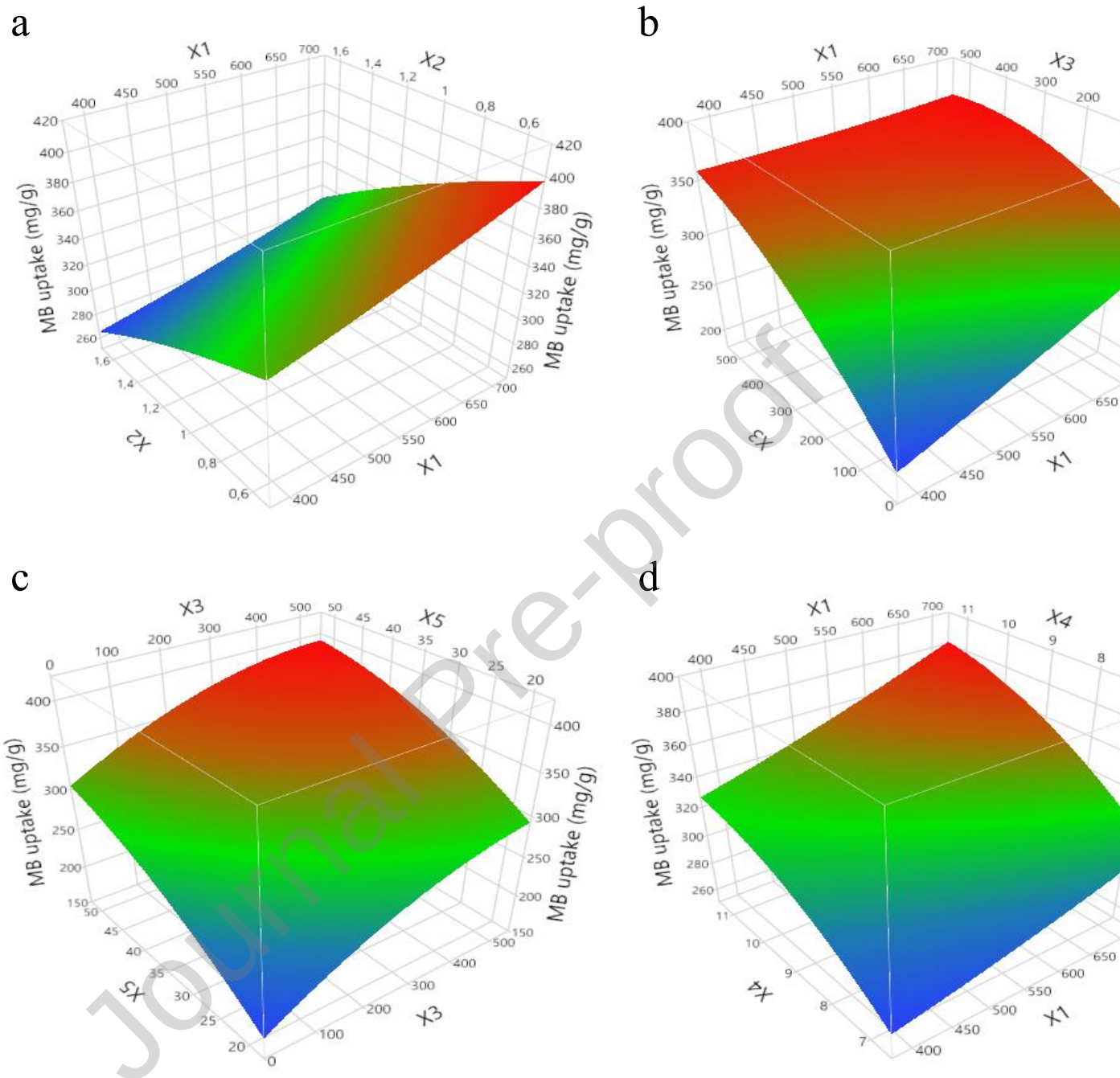

Figure 9. Response surface plot for methylene blue uptake onto the *PJAC* showing variable interactions : (a) initial MB concentration (mg/L) and *PJAC* dosage (g/L) ; (b) initial MB concentration (mg/L) and contact time (min) ; (c) contact time (min) and temperature (° C) ; (d) initial MB concentration (mg/L) and pH. In each combination, all other parameters were set to their respective mean values (initial MB concentration=550 mg/L, *PJAC* dosage= 1.1g/L, contact time= 285min, pH=9, temperature= 35°C)

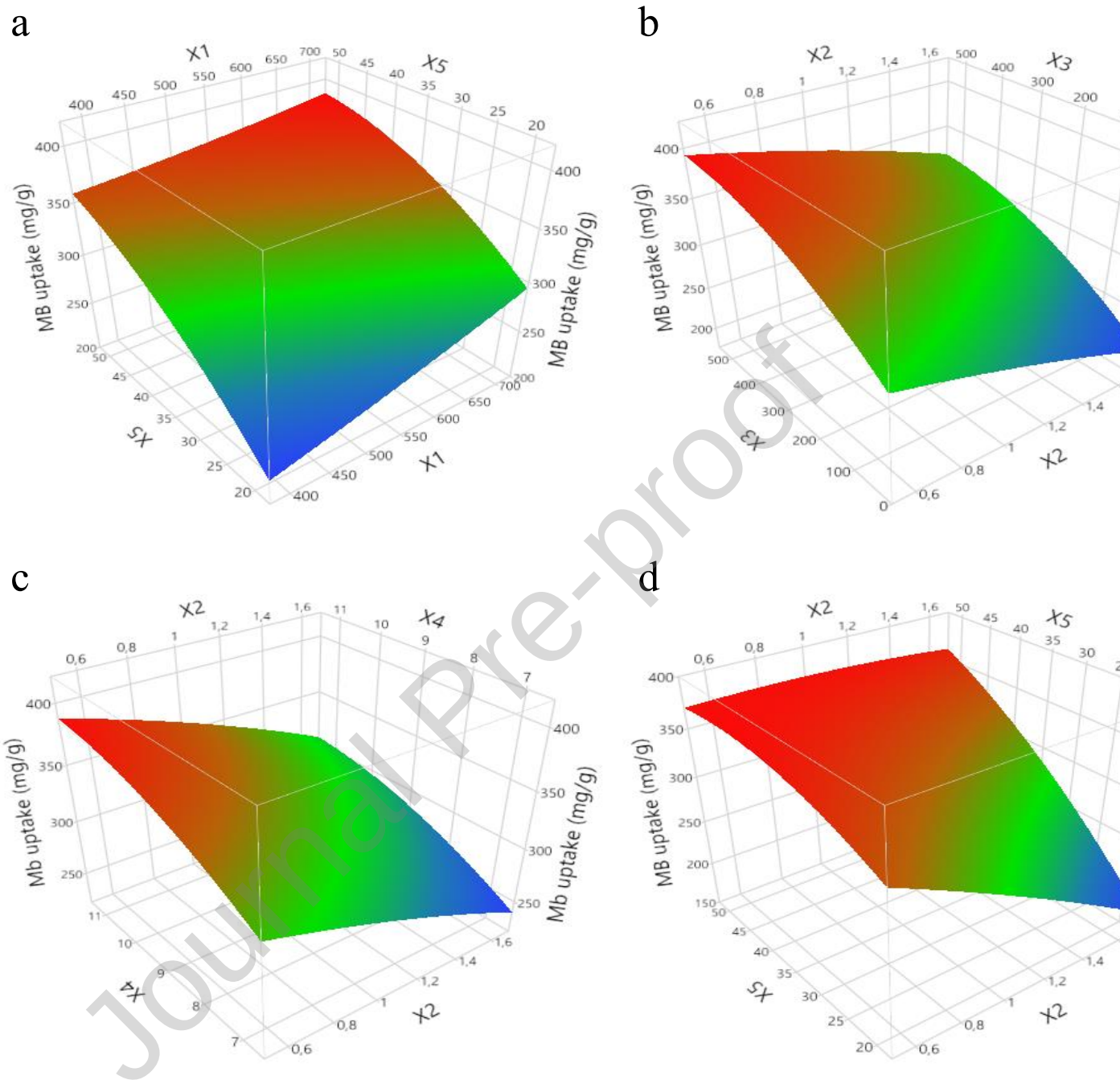

Figure 10. Response surface plot for methylene blue uptake onto the *PJAC* showing variable interactions : (a) temperature (°C) and initial MB concentration (mg/L) ; (b) contact time (min) and *PJAC* dosage (g/L) ; (c) *PJAC* dosage (g/L) and pH ; (d) *PJAC* dosage (g/L) and temperature. In each combination, all other parameters were set to their respective mean values (initial MB concentration=550 mg/L, *PJAC* dosage= 1.1g/L, contact time= 285min, pH=9, temperature= 35°C)

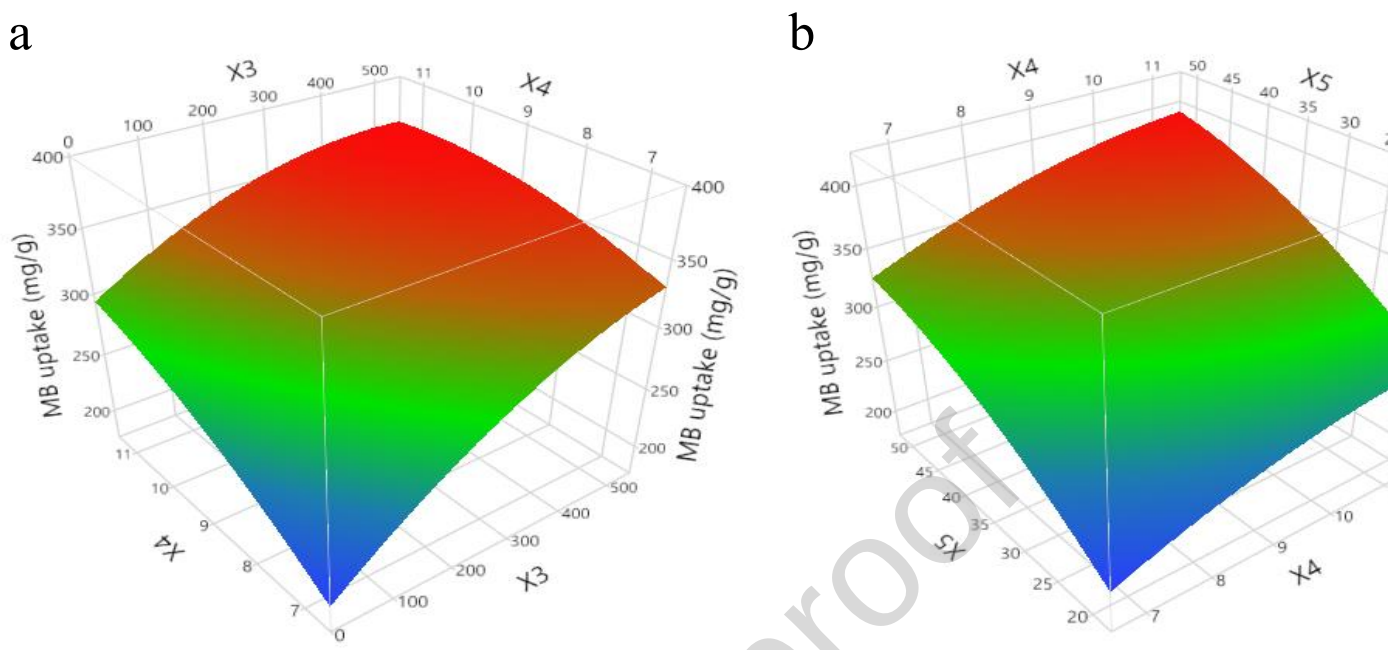

Figure 11. Response surface plot for methylene blue uptake onto the *PJAC* showing variable interactions: (a) pH and contact time (min) ; (b) pH and temperature (°C). In each combination, all other parameters were set to their respective mean values (initial MB concentration=550 mg/L, *PJAC* dosage= 1.1g/L, contact time= 285min, pH=9, temperature= 35°C)

3.5. Gaussian Process Regression model

In this work, as previously indicated to develop the GPR model (Figure 1), ten kernel functions (exponential, exponential squared, mother32, mother52, rational quadratic, exponential ard, exponential squared ard, ardmatern32, ardmatern52 and rational quadratic ard) were optimized with the basis function (constant, linear and zero).

The best model, which was obtained by optimizing kernel function, basis function and specific parameters (kernel scale and sigma), is presented in Table 11.

Table 11 shows the results of the GPR model. It shows the coefficients (R, R^2 and R_{adj}^2) and the RMSE statistical error for training, validation and all data according to specific parameters (Kernel Scale [sigmaM. sigmaF] and sigma). It also shows kernel functions with base function.

Table 11. Performance of the different GPR_DA models tested

	Kernel function	*Basis Function*	*Kernel Scale*		*Sigma*	Quantite	R/R^2/R^2_{adj}			RMSE		
			SigmaM	**SigmaF**			**Train**	**Val**	**ALL**	**Train**	**Val**	**ALL**
GPR	**ARD-Exponential**	***Constant***	42.218	123.399	2.064	35	1.000	0.916	0.994	0.385	11.977	5.866
			41.830				1.000	0.840	0.987			
			32.731				1.000	0.680	0.985			
			51.663									
			32.166									

The experimental and predicted values are graphically schematized in Figure 12.

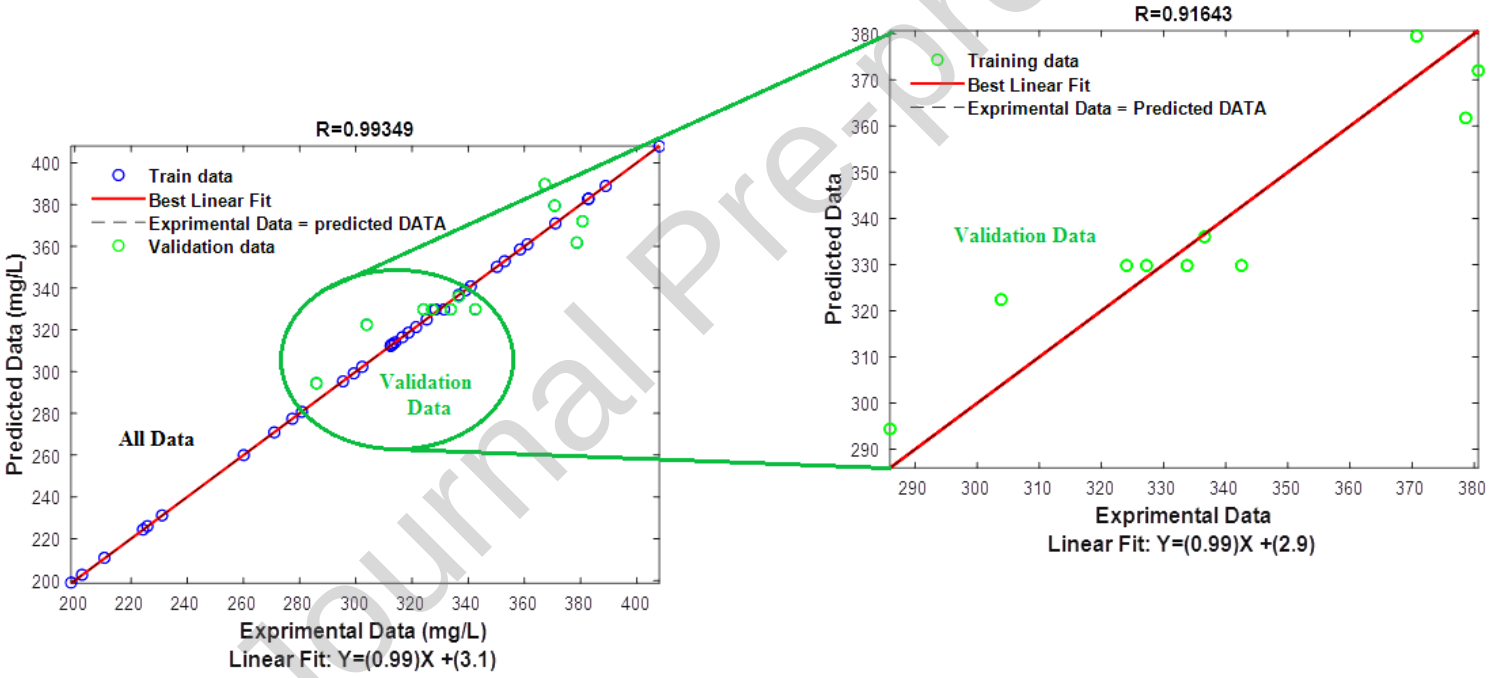

Figure 12. Comparison between experimental and predicted values

The results obtained by the GPR model show a very good performance in the learning phase and also for all the data, looking at their statistical coefficients and their errors. Indeed, the coefficients in the learning phase were 1 (R= 1.000, R^2 = 1.000 and R_{adj}^2= 1.000) and also the RMSE which was very low (RMSE= 0.385). Similarly, for all the data the coefficients were very close to 1 (R= 0.994, R^2 = 0.987 and R_{adj}^2= 0.985) and also the RMSE which was very low (RMSE= 5.866).

The problem was in the validation phase. Indeed, despite the somewhat acceptable results obtained at the level of the coefficients (R= 0.916, R^2 = 0.840 and R_{adj}^2= 0.680) and also of the RMSE (RMSE= 11.977), this remains the weak point of this model and requires further development.

3.6. Gaussian process regression model coupled with Dragonfly Algorithm (GPR_DA)

In order to improve the performance of the previously developed model, especially in the validation phase, the GPR model was coupled to the Dragonfly (DA) algorithm, which was used to optimize the specific parameters of each Kernel function, since this optimization algorithm has been used to solve a wide variety of optimization problems (Moussa et al. 2022). Among these solving different machine learning optimization problems, fundamental values and penalty parameters were optimized by the DA using training data (Moussa et al. 2022). It was confirmed by numerous studies that machine learning performance was improved when hyper-parameters were optimized using the Dragonfly algorithm (Moussa et al. 2022).

In this work, the same steps that were designed in figure 1 were performed, except that a range of optimization of number of dragonfly research agents and number of iteration (max iteration = 100 up to 500 and search agents =20 up to 50) to optimize the specific parameters of each kernel function.

The best model, which was obtained by optimizing kernel function, basis function and DA specific parameters (kernel scale and sigma) is presented in Table 12.

Table 12 shows the results of the GPR_DA model. It shows the coefficients (R, R^2 and R_{adj}^2) and the RMSE statistical error for training, validation and all data according to specific parameters (Kernel Scale [sigmaM. sigmaF] and sigma). It also shows kernel functions with base function. Note to mention, the number of dragonfly agents and the number of iterations.

Table 12. Performance of the different GPR_DA models tested

DA	Max_iteration=100 SearchAgents_no=30											
	Kernel function	***Basis Function***	***Kernel Scale***		***Sigma***	**Quantite**	**$R/R^2/R^2_{adj}$**			**RMSE**		
			SigmaM	**SigmaF**			**Train**	**Val**	**ALL**	**Train**	**Val**	**ALL**
GPR_DA	**ARD-Exponential**	***Constant***	36.709 32.882 28.037 53.931 29.150	118.801	7.172	35	0.999 0.998 0.997	0.968 0.940 0.879	0.996 0.993 0.992	2.729	7.511	4.377

The experimental and predicted values have been graphically schematized in Figure 13.

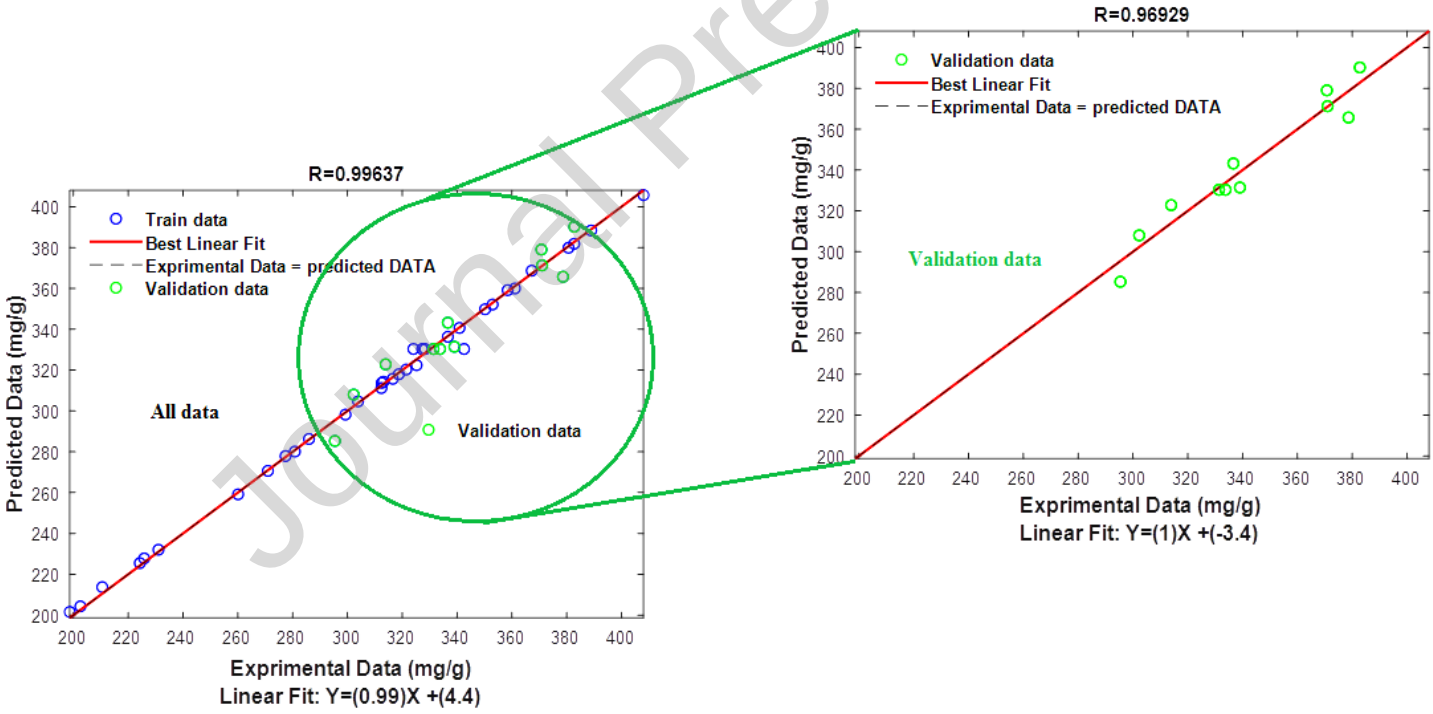

Figure 13. Comparison between experimental and predicted values

Despite the slight decrease in statistical coefficients and errors (R= 0.999, R^2=0.998, R_{adj}^2= 0.997 and RMSE= 2.729) compared to the results obtained previously by the GPR model alone during the training, but these remain very good results.

On the other hand, the results obtained by the GPR_DA model by the validation phase and all data clearly show a great improvement compared to the results obtained previously by the GPR model alone. Indeed, the coefficients in the validation phase have been improved to R= 0.968. R^2= 0.940 and R_{adj}^2= 0.879 and the RMSE has been reduced to 7.511. Similarly, for all data the coefficients became R= 0.996, R^2= 0.993 and R_{adj}^2= 0.992 and the RMSE = 4.377. From the results, it is evident that the DA optimization algorithm has improved the performance efficiency. This clearly shows the benefit of using DA algorithm.

Despite the results have been improved and have become acceptable in the validation phase (R= 0.968. R^2= 0.940, R_{adj}^2= 0.879 and RMSE = 7.511), but this requires even more an evolution of the validation phase performance in particular.

3.7. Performance development of the GPR_DA Model using Bagging (Bootstrap Aggregation_Bag):

In order to develop the validation performance of the GPR_DA model, the Bagging (Bootstrap Aggregation_Bag) technique was considered. This technique resamples the original training data set to form n different training data sets (Tahraoui et al. 2022a; Tahraoui et al. 2022b). Consequently, some of the original data points may appear more than once, while others do not appear at all in a particular replication (Tahraoui et al. 2022a; Tahraoui et al. 2022b). After training and creating the model of each training dataset that was created by GPR_DA, validation datasets were tested (Tahraoui et al. 2022a; Tahraoui et al. 2022b). Finally, an optimization number of learning Bootstrap cycle (10:30) was performed by calculating the average of predicted values of each validation by equation 17 (Tahraoui et al. 2022a; Tahraoui et al. 2022b):

$$y^{GPR\_DA\_Bootstrap\_DA} = \frac{\sum_{i=1}^{n} y_i^{IGPR\_DA}}{n} \quad (17)$$

Where, GPR_DA_Bootstrap represents Gaussian process regression coupled with Bootstrap Aggregation-Bag and Dragonfly Algorithm. IGPR_DA represents Individual Gaussian process regression (IGPR) coupled with Dragonfly Algorithm, $y_i^{IGPR\_DA}$ is the predicted output from the i[th] IGPR_DA. $y^{GPR\_DA\_Bootstrap}$ represents the predicted output from the GPR_DA_Bootstrap. and n is the number of IGPR_DA models.

The results of the training data which have been resampled for n from 1 up to 30 and the results of their validation are collected in the following table in terms of correlation coefficient and the statistical error RMSE.

Table 13. Structures of the optimized IGPR coupled with DA

DA	**Max_iteration=100** **SearchAgents_no=30**						
	Kernel function	***Basis Function***	**Quantite**	**R**		**RMSE**	
				Train	**VAL**	**Train**	**VAL**
IGPR_DA 1	**ARD-Exponential**	**Constant**	**35**	1.000	0.977	0.006	6.770
IGPR_DA 2				0.999	0.979	2.133	7.046
IGPR_DA 3				1.000	0.991	0.351	4.016
IGPR_DA 4				0.998	0.981	3.217	5.818
IGPR_DA 5				1.000	0.980	0.287	6.700
IGPR_DA 6				1.000	0.969	0.880	7.235
IGPR_DA 7				0.999	0.963	2.337	7.991
IGPR_DA 8				1.000	0.981	0.366	6.532
IGPR_DA 9				0.999	0.981	2.415	6.379

IGPR_DA 10				1.000	0.992	1.013	4.854
IGPR_DA 11				1.000	0.998	0.007	2.883
IGPR_DA 12				0.999	0.990	2.628	4.992
IGPR_DA 13				1.000	0.998	1.452	2.049
IGPR_DA 14				0.999	0.955	2.430	9.527
IGPR_DA 15				1.000	0.976	0.008	6.975
IGPR_DA 16				0.999	0.974	2.586	7.178
IGPR_DA 17				1.000	0.998	0.757	1.925
IGPR_DA 18				1.000	0.982	1.190	6.802
IGPR_DA 19				1.000	0.981	1.558	6.453
IGPR_DA 20				1.000	0.967	1.412	8.292
IGPR_DA 21				0.999	0.976	2.653	8.292
IGPR_DA 22				0.999	0.960	2.288	9.665
IGPR_DA 23				1.000	0.993	0.513	3.769
IGPR_DA 24				1.000	0.975	0.655	13.588
IGPR_DA 25				0.999	0.996	2.355	3.307
IGPR_DA 26				0.999	0.977	1.562	7.143
IGPR_DA 27				0.999	0.984	1.834	6.124
IGPR_DA 28				1.000	0.9958	0.464	3.258
IGPR_DA 29				1.000	0.985	0.769	5.053
IGPR_DA 30				1.000	0.992	1.837	4.659
$\sum_{1}^{13} y^{GPR\_DA\_Boostrap}$				/	0.994 0.988 0.975	/	3.403

In order to obtain the best result, the optimization of the average calculation of the predicted values by each number of learning Bootstrap cycle using equation 17, showed that the average of the predicted values which were obtained by the industrial models from 1 to 13 gave a very interesting result (R= 0.995, R^2= 0.991, R_{adj}^2= 0.982 and RMSE =2.949). This result is presented graphically in Figure 14.

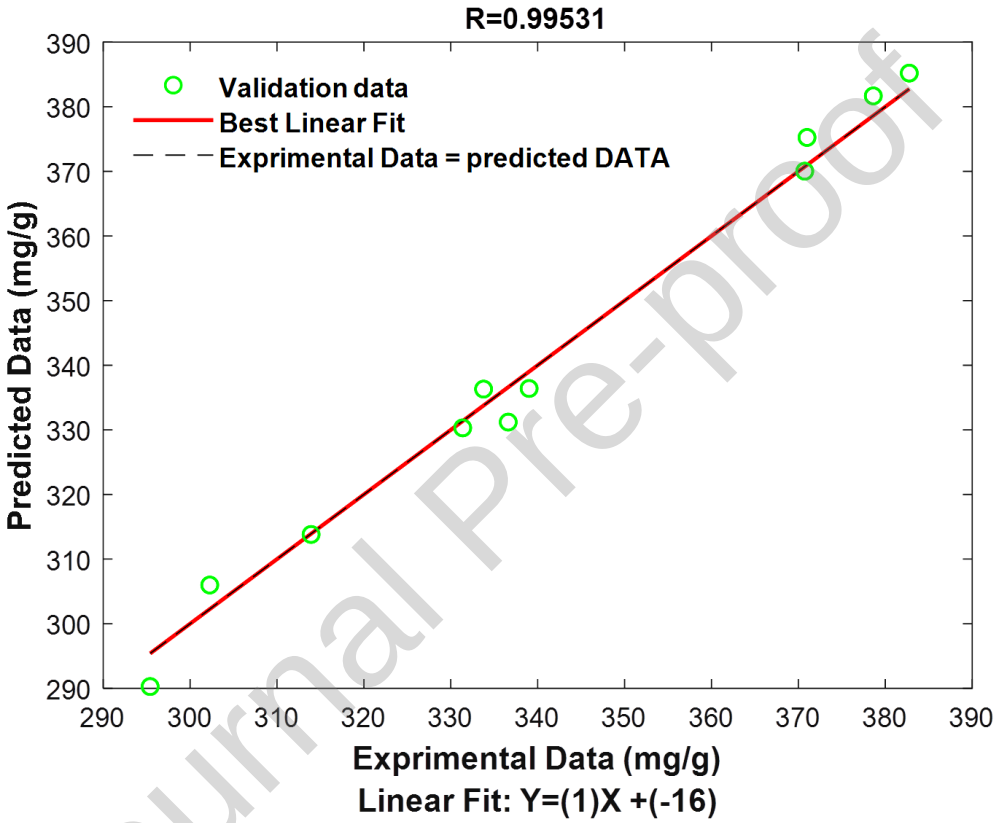

Figure 14. Comparison between experimental validation and predicted values

By comparing the results of R and RMSE, in particular for the validation phase, obtained by GPR_DA and GPR_DA_Bootstrap, it can be concluded that the Bootstrap technique developed is appropriate to enhance the performances of the GPR_DA model.

3.8. Optimization the optimal analysis

An optimization method was run using the Dragonfly Algorithm (DA in MATLAB code) and the Particle Swarm Algorithm (PSO in MATLAB code) which are available in the MATLAB

Optimization Toolbox to find the optimum of the independent parameters to obtain maximum MB uptake. The resulting solution values of this optimization are given in Table 14.

Table 14. Results of MB uptake under optimal conditions

BBD	
• DA and PSO: (X_1 = 700 mg/L. X_2 = 0.6 g/L. X_3= 490.65 min. X_4= 11. and X_5=47.89°C)	
MB uptake (mg/g). predicted values	433.81
GPR_DA_Bootstrap	
• DA and PSO: (X_1 = 700 mg/L. X_2 = 0.6 g/L. X_3= 540 min. X_4= 11. and X_5=50°C)	
MB uptake (mg/g). predicted values	492.37

The optimization analysis methods used (DA and PSO) gave the same optimization results for each model (BBD and GPR_DA_Bootstrap). This shows the reliability of the models and the quality of the experimental results obtained.

On the other hand, by comparing the results of optimization using the BBD model and the GPR_DA_Bootstrap model, it can be noted the results obtained for X_1, X_2 and X_4 are identical for the two models; while there was some difference for X_3 and a slight difference for X_5. Indeed, the contact time (X_3) in the BBD model was 490.65 min and in the GPR_DA_Bootstrap model it was 540 min. Likewise, for the temperature (X_5) it was 47.89°C and 50°C for GPR_DA_Bootstrap.

In addition, by comparing the optima obtained from each model, the GPR_DA_Bootstrap model gave a predicted value of MB uptake (492.37 mg/g) higher than that obtained by BBD (433.81 mg/g). This shows the superiority of the GPR_DA_Bootstrap model over the BBD. To confirm these results, an experimental validation method was applied.

3.9. Validation of the optimum conditions

To validate the optimization results, experiments were performed under the obtained optimal conditions to test the effectiveness of the optimization based on BBD and GPR_DA_Bootstrap. These results are presented in Table 15 in order to compare them to the predicted values and to express the error between them.

Where: $Error = Experimental\ response - Predicted\ response$ (18)

Table 15. Comparison between actual and predicted responses at optimum conditions.

BBD	
• X_1 = 700 mg/L. X_2 = 0.6 g/L. X_3 = 490.65 min. X_4 = 11. and X_5 = 47.89°C	
MB uptake (mg/g). experimental values	456.00
MB uptake (mg/g). predicted values	433.81
Error	22.19
GPR_DA_Bootstrap	
• X_1 = 700 mg/L. X_2 = 0.6 g/L. X_3 = 540 min. X_4 = 11. and X_5 = 50°C	
MB uptake (mg/g). experimental values	501.01
MB uptake (mg/g). predicted values	492.37
Error	8.64

From Table 15, it was found that the optimal conditions of the GPR_DA_Bootstrap model (X_1 = 700 mg/L, X_2 = 0.6, X_3= 540, X_4= 11 and X_5=50) gave a result of MB uptake (501.01 mg/g), which is significantly higher than that given by the BBD model (456mg/g). In addition, the error obtained by the GPR_DA_Bootstrap model (8.64 mg/g) was lower than that obtained by the BBD (22.19 mg/g). This clearly shows the superiority of the GPR_DA_Bootstrap model. However, the BBD model was also effective and performing,

owing to the result that was obtained (456.00 mg/g) under optimal conditions (X_1 = 700 mg/L, X_2 = 0.6 g/L, X_3 = 490.65 min, X_4 = 11 and X_5 = 47.89°C).

3.10. Interface for optimization and prediction

To provide a simple way to implement optimal optimization and predict MB uptake, an interface was designed using the MATLAB guide for optimization and prediction (Figure 15). This interface was converted into an executable application on Windows. This powerful application for direct use allows to predict the outputs by selecting the input values by BBD, as well asby GPR__DA_Bootstrap. Moreover, the application is also an optimization solution, allowing finding the optimal ones for each type of model (BBD and GPR_DA_Bootstrap) by two methods (DA and PSO).

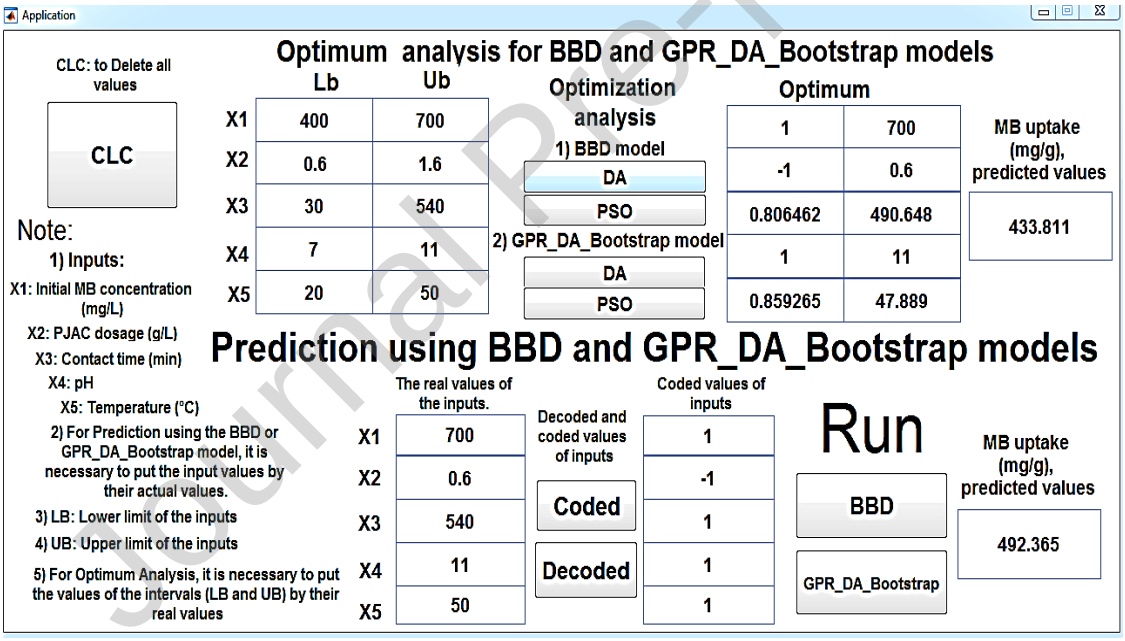

Figure 15. MATLAB Interface for optimization analysis (DA and PSO) and prediction of MB uptake using BBD and GPR_DA_Bootstrap.

3.11. Adsorption mechanism

The thermodynamics parameters study revealed that MB adsorption capacity was positively influenced by temperature, this may be due to the decrease in the viscosity of the solution and the increment of the MB molecules mobility with increasing temperature, leading to an

increase in the adsorption (Khan et al. 2020; Li et al. 2020). The results also showed that the adsorption of MB on the *PJAC* followed a physisorption mechanism. the main suggested interactions between *PJAC* and MB were electrostatic, dipole-dipole interactions and hydrogen bonding (Üner et al. 2016). Figure 16 represents the main interactions and MB possible adsorption mechanisms involved in the sorption process. Boehm titration and FTIR analysis showed the presence of functional groups on the surface of *PJAC* and their involvement in the adsorption process (O-H, COOH, N-H, C-O-C and C-O bands). It has also confirmed in this study that the adsorption of methylene blue on the *PJAC* was highly influenced by the pH of the solution and pH_{pzc}. The *PJAC* surface is negatively charged at solution pH higher then pH_{pzc}, which enhances the MB adsorption simply by electrostatic forces onto negatively charged *PJAC* surface as shown in Figure 16. The Methylene blue can also be easily adsorbed onto *PJAC* by the π-π stacking interaction that occur between the π–electron system of the activated carbon and the aromatic rings of the MB dye molecules (Jawad et al. 2020b). The third type of interaction that can be expected to occur is the hydrogen bonding between the nitrogen of MB molecules and the hydrogen band of phenolic and carboxylic functions (Mbarki et al. 2022). Similar findings regarding the MB adsorption by activated carbon-based adsorbents were proposed in the literature (Üner et al. 2016; Jawad et al. 2019; Jawad et al. 2020b; Jawad et al. 2021; Jawad et al. 2022; Mbarki et al. 2022).

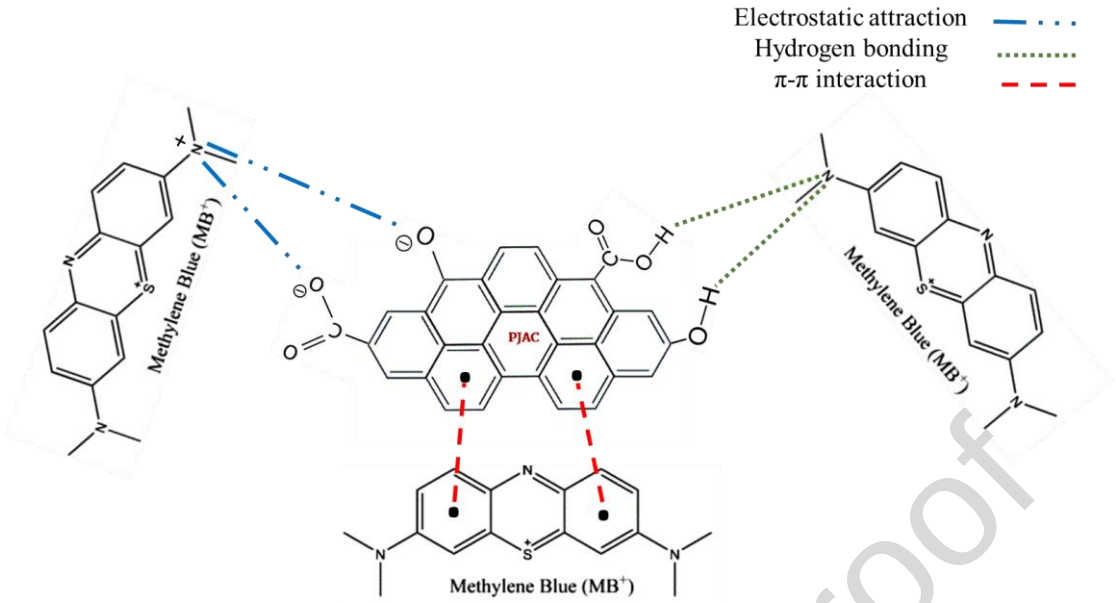

Figure 16. Illustration of the possible interaction between *PJAC* and MB molecules dye

4. Conclusion

Activated carbon prepared from jujube stones (*PJAC*) was used successfully as a low-cost adsorbent to remove methylene blue. The MB adsorption met Langmuir isotherm model with maximum adsorption capacity of 387.606 mg/g in test conditions (adsorbent dosage=1.00 g/L, Time=540min, T=25°C and pH=7, agitation rate=200 rpm). The pseudo-second order model has better described the sorption phenomenon. The thermodynamic and mechanism studies revealed that the MB adsorption was spontaneous, endothermic and mainly of physical nature and carried out by surface interactions, such as electrostatics, H-bonds and π-π stacking interactions. The response surface approach with Box Behnken design method and Gaussian process regression coupled with bagging (Bootstrap Aggregation_Bag) and Dragonfly optimization algorithm (GPR_DA_Bootstrap) were used to improve the independent process parameters. The optimal conditions using the BBD model were found to be an initial methylene blue concentration of 700 mg/L, adsorbent dose of 0.6 g/L, contact time of 490.65 min, pH of 11 and a temperature of 47.89°C, leading to an adsorption of 456.00 mg/g of MB. On the other hand, the efficiency of the GPR_DA_Bootstrap model led to 501.01 mg/g MB uptake for an initial MB amount of 700 mg/L, 0.6 g/L adsorbent dosage, 540 min contact

time, a pH of 11 and a temperature of 50°C. From the obtained results, it can be deduced that the GPR_DA_Bootstrap model is more efficient than the BBD model, and also that the Jujube stone based prepared activated carbon can be effectively used as an available, economical adsorbent with high adsorption capacity and good affinity to cationic dyes.

Declaration of interests

☒The authors declare that they have no known competing financial interests or personal relationships that could have appeared to influence the work reported in this paper.

☐The authors declare the following financial interests/personal relationships which may be considered as potential competing interests:

References:

Ab Ghani Z, Yusoff MS, Zaman NQ, Zamri MFMA, Andas J. 2017. Optimization of preparation conditions for activated carbon from banana pseudo-stem using response surface methodology on removal of color and COD from landfill leachate. *Waste Management* **62**: 177-187. https://doi.org/10.1016/j.wasman.2017.02.026

Abbas M. 2021. Modeling of adsorption isotherms of heavy metals onto Apricot stone activated carbon: two-parameter models and equations allowing determination of thermodynamic parameters. *Materials Today: Proceedings* **43**: 3359-3364. https://doi.org/10.1016/j.matpr.2020.05.320

Abdulhameed AS, Hum NNMF, Rangabhashiyam S, Jawad AH, Wilson LD, Yaseen ZM, Al-Kahtani AA, ALOthman ZA. 2021. Statistical modeling and mechanistic pathway for methylene blue dye removal by high surface area and mesoporous grass-based activated carbon using K_2CO_3 activator. *Journal of Environmental Chemical Engineering* **9**: 105530. https://doi.org/10.1016/j.jece.2021.105530

Abdulhameed AS, Mohammad A, Jawad AH. 2019. Modeling and mechanism of reactive orange 16 dye adsorption by chitosan-glyoxal/TiO_2 nanocomposite: application of response surface methodology. *Desalination and Water Treatment* **164**: 346-360. https://doi:10.5004/dwt.2019.24384

Ahmed MJ, Dhedan SK. 2012. Equilibrium isotherms and kinetics modeling of methylene blue adsorption on agricultural wastes-based activated carbons. *Fluid phase equilibria* **317**: 9-14. https://doi.org/10.1016/j.fluid.2011.12.026

Alhalili Z. 2022. Green synthesis of copper oxide nanoparticles CuO NPs from Eucalyptus Globoulus leaf extract: Adsorption and design of experiments. *Arabian Journal of Chemistry* **15**: 103739. https://doi.org/10.1016/j.arabjc.2022.103739

Aminu I, Gumel SM, Ahmad WA, Idris AA. 2020. Adsorption isotherms and kinetic studies of Congo-red removal from waste water using activated carbon prepared from jujube seed. *American Journal of Analytical Chemistry* **11**: 47. https://doi.org/10.4236/ajac.2020.111004

Angın D. 2013. Effect of pyrolysis temperature and heating rate on biochar obtained from pyrolysis of safflower seed press cake. *Bioresource technology* **128**: 593-597. https://doi.org/10.1016/j.biortech.2012.10.150

Aravind M, Amalanathan M, Mary M, Parvathiraja C, Alothman AA, Wabaidur SM, Islam MA. 2022. Enhanced photocatalytic and biological observations of green synthesized activated carbon, activated carbon doped silver and activated carbon/silver/titanium dioxide nanocomposites. *Journal of Inorganic and Organometallic Polymers and Materials* **32**: 267-279. https://doi.org/10.1007/s10904-021-02096-w

Asfaram A, Ghaedi M, Azqhandi MA, Goudarzi A, Dastkhoon M. 2016. Statistical experimental design, least squares-support vector machine (LS-SVM) and artificial neural network (ANN) methods for modeling the facilitated adsorption of methylene blue dye. *RSC advances* **6**: 40502-40516. https://doi.org/10.1039/c6ra01874b

Bahnes Z, Benderdouche N, Attouti S, Bestani B, Duclaux L, Reinert L. 2018. Preparation of a novel activated carbon from jujube stones (Ziziphus jujuba) for the removal of basic and acid dyes. *Desalination and Water Treatment* **102**: 312-325. https://doi.org/10.5004/dwt.2018.21854

Baidya KS, Kumar U. 2021. Adsorption of brilliant green dye from aqueous solution onto chemically modified areca nut husk. *South African Journal of Chemical Engineering* **35**: 33-43. https://doi.org/10.1016/j.sajce.2020.11.001

Bangari RS, Yadav A, Bharadwaj J, Sinha N. 2022. Boron nitride nanosheets incorporated polyvinylidene fluoride mixed matrix membranes for removal of methylene blue from aqueous stream. Journal of Environmental Chemical Engineering 10: 107052. https://doi.org/10.1016/j.jece.2021.107052

Belsley DA, Kuh E, Welsch RE. 2005. *Regression diagnostics: Identifying influential data and sources of collinearity*. John Wiley & Sons.

Benadjemia M, Millière L, Reinert L, Benderdouche N, Duclaux L. 2011. Preparation, characterization and Methylene Blue adsorption of phosphoric acid activated carbons from globe artichoke leaves. *Fuel Processing Technology* **92**: 1203-1212. https://doi.org/10.1016/j.fuproc.2011.01.014

Bencheikh I, Azoulay K, Mabrouki J, El Hajjaji S, Moufti A, Labjar N. 2021. The use and the performance of chemically treated artichoke leaves for textile industrial effluents treatment. *Chemical Data Collections* **31**: 100597. https://doi.org/10.1016/j.cdc.2020.100597

Bohli T, Ouederni A, Fiol N, Villaescusa I. 2015. Evaluation of an activated carbon from olive stones used as an adsorbent for heavy metal removal from aqueous phases. *Comptes rendus chimie* **18**: 88-99. https://doi.org/10.1016/j.crci.2014.05.009

Bouchelkia N, Mouni L, Belkhiri L, Bouzaza A, Bollinger J-C, Madani K, Dahmoune F. 2016. Removal of lead (II) from water using activated carbon developed from jujube stones, a low-cost sorbent. *Separation Science and Technology* **51**: 1645-1653. https://doi.org/10.1080/01496395.2016.1178289

Boudechiche N, Fares M, Ouyahia S, Yazid H, Trari M, Sadaoui Z. 2019. Comparative study on removal of two basic dyes in aqueous medium by adsorption using activated carbon from Ziziphus lotus stones. *Microchemical Journal* **146**: 1010-1018. https://doi.org/10.1016/j.microc.2019.02.010

Bousselma A, Abdessemed D, Tahraoui H, Amrane A. 2021. Artificial intelligence and mathematical modelling of the drying kinetics of pre-treated whole apricots. *Kemija u industriji* **70**: 651-667. https://doi.org/10.15255/KUI.2020.079

Box GE, Behnken DW. 1960. Some new three level designs for the study of quantitative variables. *Technometrics* **2**: 455-475.

Chedri Mammar A, Mouni L, Bollinger J-C, Belkhiri L, Bouzaza A, Assadi AA, Belkacemi H. 2020. Modeling and optimization of process parameters in elucidating the adsorption mechanism

of Gallic acid on activated carbon prepared from date stones. *Separation Science and Technology* **55**: 3113-3125. https://doi.org/10.1080/01496395.2019.1676785

Chen H, Zhao J, Dai G. 2011. Silkworm exuviae—A new non-conventional and low-cost adsorbent for removal of methylene blue from aqueous solutions. Journal of hazardous materials 186: 1320-1327. https://doi.org/10.1016/j.jhazmat.2010.12.006

Cheng T, Li J, Ma X, Zhou L, Wu H, Yang L. 2021. The adsorption properties of microporous activated carbon prepared from pistachio nut shell for low-concentration VOCs under low-medium temperatures. *Environmental Science and Pollution Research* **28**: 65216–65228 https://doi.org/10.1007/s11356-021-14586-y

Dao MU, Le HS, Hoang HY, Tran VA, Doan VD, Le TTN, Sirotkin A. 2021. Natural core-shell structure activated carbon beads derived from Litsea glutinosa seeds for removal of methylene blue: Facile preparation, characterization, and adsorption properties. *Environmental Research* **198**: 110481. https://doi.org/10.1016/j.envres.2020.110481

Daoud M, Benturki O, Girods P, Donnot A, Fontana S. 2019. Adsorption ability of activated carbons from Phoenix dactylifera rachis and Ziziphus jujube stones for the removal of commercial dye and the treatment of dyestuff wastewater. *Microchemical Journal* **148**: 493-502. https://doi.org/10.1016/j.microc.2019.05.022

Das D, Das N. 2014. Optimization of parameters for cerium (III) biosorption onto biowaste materials of animal and plant origin using 5-level Box-Behnken design: Equilibrium, kinetic, thermodynamic and regeneration studies. *Journal of Rare Earths* **32**: 745-758. https://doi.org/10.1016/S1002-0721(14)60136-8

de Souza CC, de Souza LZM, Yılmaz M, de Oliveira MA, da Silva Bezerra AC, da Silva EF, Dumont MR, Machado ART. 2022. Activated carbon of Coriandrum sativum for adsorption of methylene blue: Equilibrium and kinetic modeling. *Cleaner Materials* **3**: 100052. https://doi.org/10.1016/j.clema.2022.100052

Dotto G, Santos J, Rodrigues I, Rosa R, Pavan F, Lima E. 2015. Adsorption of methylene blue by ultrasonic surface modified chitin. *Journal of colloid and interface science* **446**: 133-140. https://doi.org/10.1016/j.jcis.2015.01.046

Douara N, Bestani B, Benderdouche N, Duclaux L. 2016. Sawdust-based activated carbon ability in the removal of phenol-based organics from aqueous media. *Desalination and Water Treatment* **57**: 5529-5545. https://doi.org/10.1080/19443994.2015.1005151

Du C, Liu B, Hu J, Li H. 2021. Determination of iodine number of activated carbon by the method of ultraviolet–visible spectroscopy. *Materials Letters* **285**: 129137. https://doi.org/10.1016/j.matlet.2020.129137

El Nemr A, Shoaib AG, El Sikaily A, Mohamed AE-DA, Hassan AF. 2021. Evaluation of Cationic Methylene Blue Dye Removal by High Surface Area Mesoporous Activated Carbon Derived from Ulva lactuca. *Environmental Processes* **8**: 311-332. https://doi.org/10.1007/s40710-020-00487-8

Ferreira LM, de Melo RR, Pimenta AS, de Azevedo TKB, de Souza CB. 2020. Adsorption performance of activated charcoal from castor seed cake prepared by chemical activation with phosphoric acid. Biomass Conversion and Biorefinery **12:** 1181–1192. https://doi.org/10.1007/s13399-020-00660-x

Ferreira SC, Bruns R, Ferreira H, Matos G, David J, Brandão G, da Silva EP, Portugal L, Dos Reis P, Souza A. 2007. Box-Behnken design: an alternative for the optimization of analytical methods. *Analytica chimica acta* **597**: 179-186. https://doi.org/10.1016/j.aca.2007.07.011

Gao J, Liu Y, Li X, Yang M, Wang J, Chen Y. 2020. A promising and cost-effective biochar adsorbent derived from jujube pit for the removal of Pb (II) from aqueous solution. *Scientific reports* **10**: 1-13. https://doi.org/10.1016/j.envres.2020.110481

Ghosh A, Das P, Sinha K. 2015. Modeling of biosorption of Cu (II) by alkali-modified spent tea leaves using response surface methodology (RSM) and artificial neural network (ANN). Applied Water Science **5**: 191-199. https://doi.org/10.1007/s13201-014-0180-z

Giraldo S, Robles I, Godínez LA, Acelas N, Flórez E. 2021. Experimental and theoretical insights on methylene blue removal from wastewater using an adsorbent obtained from the residues of the orange industry. *Molecules* **26**: 4555. https://doi.org/10.3390/molecules26154555

González-Crisostomo JC, López-Juárez R, Yocupicio-Gaxiola RI, Villanueva E, Zavala-Flores E, Petranovskii V. 2022. Chabazite Synthesis and Its Exchange with Ti, Zn, Cu, Ag and Au for Efficient Photocatalytic Degradation of Methylene Blue Dye. *International Journal of Molecular Sciences* **23**: 1730. https://doi.org/10.3390/ijms23031730

Guarín-Romero JR, Rodríguez-Estupiñán P, Giraldo L, Moreno-Piraján JC. 2019. Simple and competitive adsorption study of nickel (II) and chromium (III) on the surface of the brown algae Durvillaea antarctica biomass. *ACS omega* **4**: 18147-18158. https://doi.org/10.1021/acsomega.9b02061

Han C, Pu H, Li H, Deng L, Huang S, He S, Luo Y. 2013. The optimization of As (V) removal over mesoporous alumina by using response surface methodology and adsorption mechanism. *Journal of hazardous materials* **254**: 301-309. https://doi.org/10.1016/j.jhazmat.2013.04.008

Han Q, Wang J, Goodman BA, Xie J, Liu Z. 2020. High adsorption of methylene blue by activated carbon prepared from phosphoric acid treated eucalyptus residue. *Powder Technology* **366**: 239-248. https://doi.org/10.1016/j.powtec.2020.02.013

Hang PT, Brindley G. 1970. Methylene blue absorption by clay minerals. Determination of surface areas and cation exchange capacities (clay-organic studies XVIII). *Clays and clay minerals* **18**: 203-212. https://doi.org/10.1346/CCMN.1970.0180404

Helm JM, Swiergosz AM, Haeberle HS, Karnuta JM, Schaffer JL, Krebs VE, Spitzer AI, Ramkumar PN. 2020. Machine learning and artificial intelligence: definitions, applications, and future directions. Current reviews in musculoskeletal medicine **13**: 69-76. https://doi.org/10.1007/s12178-020-09600-8

Hesas RH, Arami-Niya A, Daud WMAW, Sahu J. 2013. Preparation and characterization of activated carbon from apple waste by microwave-assisted phosphoric acid activation: application in methylene blue adsorption. *BioResources* **8**: 2950-2966.

Heschel W, Klose E. 1995. On the suitability of agricultural by-products for the manufacture of granular activated carbon. *Fuel* **74**: 1786-1791. https://doi.org/10.1016/0016-2361(95)80009-7

Hong SH, Lee MW, Lee DS, Park JM. 2007. Monitoring of sequencing batch reactor for nitrogen and phosphorus removal using neural networks. *Biochemical Engineering Journal* **35**: 365-370. https://doi.org/10.1016/j.bej.2007.01.033

Huang Y, Zhu J, Liu H, Wang Z, Zhang X. 2019. Preparation of porous graphene/carbon nanotube composite and adsorption mechanism of methylene blue. SN Applied Sciences **1**: 37. https://doi.org/10.1007/s42452-018-0035-6

Ihaddaden S, Aberkane D, Boukerroui A, Robert D. 2022. Removal of methylene blue (basic dye) by coagulation-flocculation with biomaterials (bentonite and Opuntia ficus indica). Journal of Water Process Engineering **49**: 102952. https://doi.org/10.1016/j.jwpe.2022.102952

Jawad AH, Abd Malek NN, Khadiran T, ALOthman ZA, Yaseen ZM. 2022. Mesoporous high-surface-area activated carbon from biomass waste via microwave-assisted-H_3PO_4 activation for methylene blue dye adsorption: An optimized process. *Diamond and Related Materials* **128**: 109288. https://doi.org/10.1016/j.diamond.2022.109288

Jawad AH, Abdulhameed AS, Wilson LD, Syed-Hassan SSA, ALOthman ZA, Khan MR. 2021. High surface area and mesoporous activated carbon from KOH-activated dragon fruit peels for methylene blue dye adsorption: Optimization and mechanism study. Chinese Journal of Chemical Engineering **32**: 281-290. https://doi.org/10.1016/j.cjche.2020.09.070

Jawad AH, Bardhan M, Islam MA, Islam MA, Syed-Hassan SSA, Surip S, ALOthman ZA, Khan MR. 2020a. Insights into the modeling, characterization and adsorption performance of mesoporous activated carbon from corn cob residue via microwave-assisted H_3PO_4 activation. *Surfaces and interfaces* **21**: 100688. https://doi.org/10.1016/j.surfin.2020.100688

Jawad AH, Ismail K, Ishak MAM, Wilson LD. 2019. Conversion of Malaysian low-rank coal to mesoporous activated carbon: structure characterization and adsorption properties. *Chinese Journal of Chemical Engineering* **27**: 1716-1727. https://doi.org/10.1016/j.cjche.2018.12.006

Jawad AH, Kadhum AM, Ngoh Y. 2018a. Applicability of dragon fruit (Hylocereus polyrhizus) peels as low-cost biosorbent for adsorption of methylene blue from aqueous solution: kinetics, equilibrium and thermodynamics studies. *Desalin Water Treat* **109**: 231-240. https://doi.org/10.5004/dwt.2018.21976

Jawad AH, Mohammed SA, Mastuli MS, Abdullah MF. 2018b. Carbonization of corn (Zea mays) cob agricultural residue by one-step activation with sulfuric acid for methylene blue adsorption. Desalin Water Treat **118:** 342-351. https://doi.org/10.5004/dwt.2018.22680

Jawad AH, Mohd Firdaus Hum NN, Abdulhameed AS, Mohd Ishak MA. 2020b. Mesoporous activated carbon from grass waste via H_3PO_4-activation for methylene blue dye removal: modelling, optimisation, and mechanism study. *International Journal of Environmental Analytical Chemistry*: 1-17. https://doi.org/10.1080/03067319.2020.1807529

Jawad AH, Rashid RA, Ishak MAM, Ismail K. 2018c. Adsorptive removal of methylene blue by chemically treated cellulosic waste banana (Musa sapientum) peels. Journal of Taibah University for Science **12**: 809-819. https://doi.org/10.1080/16583655.2018.1519893

Jawad AH, Surip S. 2022. Upgrading low rank coal into mesoporous activated carbon via microwave process for methylene blue dye adsorption: Box Behnken Design and mechanism study. Diamond and Related Materials **127**: 109199. https://doi.org/10.1016/j.diamond.2022.109199

Khan N, Wahid F, Sultana Q, Saqib NU, Rahim M. 2020. Surface oxidized and un-oxidized activated carbon derived from Ziziphus jujube Stem, and its application in removal of Cd (II) and Pb (II) from aqueous media. SN Applied Sciences **2**: 1-11. https://doi.org/10.1007/s42452-020-2578-6

Khoo E-C, Ong S-T, Hung Y-T, Ha S-T. 2013. Removal of basic dyes from aqueous solution using sugarcane bagasse: optimization by Plackett–Burman and Response Surface Methodology. *Desalination and Water Treatment* **51**: 7109-7119. https://doi.org/10.1080/19443994.2013.791774

Khuongab DA, Nguyen HN, Tsubota T. 2021. Activated carbon produced from bamboo and solid residue by CO_2 activation utilized as CO_2 adsorbents. *Biomass and Bioenergy* **148**: 106039. https://doi.org/10.1016/j.biombioe.2021.106039

Kibami D, Chubaakum P, Rao K, Dipak S. 2014. Preparation and characterization of activated carbon from Fagopyrum esculentum Moench by HNO_3 and H_3PO_4 chemical activation. *Der Chemica Sinica* **5**: 46-55.

Kıvanç MR, Yönten V. 2020. A statistical optimization of methylene blue removal from aqueous solutions by Agaricus Campestris using multi-step experimental design with response surface methodology: Isotherm, kinetic and thermodynamic studies. *Surfaces and interfaces* **18**: 100414. https://doi.org/10.1016/j.surfin.2019.100414

Kundu A, Gupta BS, Hashim MA, Redzwan G. 2015. Taguchi optimization approach for production of activated carbon from phosphoric acid impregnated palm kernel shell by microwave heating. *Journal of cleaner production* **105**: 420-427. https://doi.org/10.1016/j.jclepro.2014.06.093

Labied R, Benturki O, Eddine Hamitouche AY, Donnot A. 2018. Adsorption of hexavalent chromium by activated carbon obtained from a waste lignocellulosic material (Ziziphus jujuba cores): Kinetic, equilibrium, and thermodynamic study. *Adsorption science & technology* **36**: 1066-1099. https://doi.org/10.1177/0263617417750739

Lakshmi D, Akhil D, Kartik A, Gopinath KP, Arun J, Bhatnagar A, Rinklebe J, Kim W, Muthusamy G. 2021. Artificial intelligence (AI) applications in adsorption of heavy metals using modified biochar. *Science of The Total Environment* **801**: 149623. https://doi.org/10.1016/j.scitotenv.2021.149623

Li H, Budarin VL, Clark JH, North M, Wu X. 2022. Rapid and Efficient Adsorption of Methylene Blue Dye From Aqueous Solution by Hierarchically Porous, Activated Starbons®: Mechanism and Porosity Dependence. *Journal of hazardous materials* **436**: 129174. https://doi.org/10.1016/j.jhazmat.2022.129174

Li Z, Hanafy H, Zhang L, Sellaoui L, Netto MS, Oliveira ML, Seliem MK, Dotto GL, Bonilla-Petriciolet A, Li Q. 2020. Adsorption of congo red and methylene blue dyes on an ashitaba waste and a walnut shell-based activated carbon from aqueous solutions: Experiments, characterization and physical interpretations. *Chemical Engineering Journal* **388**: 124263. https://doi.org/10.1016/j.cej.2020.124263

Liou T-H. 2010. Development of mesoporous structure and high adsorption capacity of biomass-based activated carbon by phosphoric acid and zinc chloride activation. *Chemical Engineering Journal* **158**: 129-142. https://doi.org/10.1016/j.cej.2009.12.016

Liu H, Yang C, Huang M, Wang D, Yoo C. 2018. Modeling of subway indoor air quality using Gaussian process regression. *Journal of hazardous materials* **359**: 266-273. https://doi.org/10.1016/j.jhazmat.2018.07.034

Ma C, Lu T, Shao J, Huang J, Hu X, Wang L. 2022. Biomass derived nitrogen and sulfur co-doped porous carbons for efficient CO_2 adsorption. *Separation and Purification Technology* **281**: 119899. https://doi.org/10.1016/j.seppur.2021.119899

Mansouri S, Elhammoudi N, Aboul-hrouz S, Mouiya M, Makouki L, Chham A, Abourriche A, Hannache H, Oumam M. 2018. Elaboration of novel adsorbent from Moroccan oil shale using Plackett–Burman design. *Chem Int* **4**: 7-14.

Mashkoor F, Nasar A. 2020. Magsorbents: Potential candidates in wastewater treatment technology–A review on the removal of methylene blue dye. *Journal of magnetism and magnetic materials* **500**: 166408. https://doi.org/10.1016/j.jmmm.2020.166408

Mbarki F, Selmi T, Kesraoui A, Seffen M. 2022. Low-cost activated carbon preparation from Corn stigmata fibers chemically activated using H_3PO_4, $ZnCl_2$ and KOH: Study of methylene blue adsorption, stochastic isotherm and fractal kinetic. *Industrial Crops and Products* **178**: 114546. https://doi.org/10.1016/j.indcrop.2022.114546

Mehmood A, Bano S, Fahim A, Parveen R, Khurshid S. 2015. Efficient removal of crystal violet and eosin B from aqueous solution using Syzygium cumini leaves: a comparative study of acidic and basic dyes on a single adsorbent. *Korean Journal of Chemical Engineering* **32**: 882-895. https://doi.org/10.1007/s11814-014-0308-8

Mouni L, Belkhiri L, Bollinger J-C, Bouzaza A, Assadi A, Tirri A, Dahmoune F, Madani K, Remini H. 2018. Removal of Methylene Blue from aqueous solutions by adsorption on Kaolin: Kinetic and equilibrium studies. *Applied Clay Science* **153**: 38-45. https://doi.org/10.1016/j.clay.2017.11.034

Moussa H, Dahmoune F, Hentabli M, Remini H, Mouni L. 2022. Optimization of ultrasound-assisted extraction of phenolic-saponin content from Carthamus caeruleus L. rhizome and predictive model based on support vector regression optimized by dragonfly algorithm. *Chemometrics and Intelligent Laboratory Systems* **222**: 104493. https://doi.org/10.1016/j.chemolab.2022.104493

Msaada A, Belbahloula M, El Hajjajib S, Beakoua BH, Houssainia MA, Belhajjiaa C, Aassilac H, Zouhria A, Anouara A. 2018. Industrial wastewater decolorization by activated carbon from Ziziphus lotus. *Desalin Water Treat* **126**: 296-305. https://doi.org/10.5004/dwt.2018.22904

Onu CE, Nwabanne JT, Ohale PE, Asadu CO. 2021. Comparative analysis of RSM, ANN and ANFIS and the mechanistic modeling in eriochrome black-T dye adsorption using modified clay. *South African Journal of Chemical Engineering* **36**: 24-42. https://doi.org/10.1016/j.sajce.2020.12.003

Panadare DC, Lade VG, Rathod VK. 2014. Adsorptive removal of copper (II) from aqueous solution onto the waste sweet lime peels (SLP): equilibrium, kinetics and thermodynamics studies. Desalination and Water Treatment 52: 7822-7837. https://doi.org/10.1080/19443994.2013.831789

Pandey S, Fosso-Kankeu E, Ramontja J. 2017. Efficient and rapid adsorption characteristics of templating xanthan gum-graft-poly (aniline) and silica nanocomposite toward removal of toxic methylene blue dyes. in *9th International Conference on Advances in Science, Engineering, Technology and Waste Management (ASETWM-2017)*, pp. 27-28. https://doi.org/10.17758/EARES.EAP1117052

Park J, Lechevalier D, Ak R, Ferguson M, Law KH, Lee Y-T, Rachuri S. 2017. Gaussian process regression (GPR) representation in predictive model markup language (PMML). *Smart and sustainable manufacturing systems* **1**: 121-141. https://doi.org/10.1520/SSMS20160008

Peñafiel ME, Matesanz JM, Vanegas E, Bermejo D, Mosteo R, Ormad MP. 2021. Comparative adsorption of ciprofloxacin on sugarcane bagasse from Ecuador and on commercial powdered activated carbon. *Science of The Total Environment* **750**: 141498. https://doi.org/10.1016/j.scitotenv.2020.141498

Postai DL, Demarchi CA, Zanatta F, Melo DCC, Rodrigues CA. 2016. Adsorption of rhodamine B and methylene blue dyes using waste of seeds of Aleurites Moluccana, a low cost adsorbent. *Alexandria Engineering Journal* **55**: 1713-1723. https://doi.org/10.1016/j.aej.2016.03.017

Prahas D, Kartika Y, Indraswati N, Ismadji S. 2008. Activated carbon from jackfruit peel waste by H3PO4 chemical activation: Pore structure and surface chemistry characterization. *Chemical Engineering Journal* **140**: 32-42. https://doi.org/10.1016/j.cej.2007.08.032

Ren Z, Jia B, Zhang G, Fu X, Wang Z, Wang P, Lv L. 2021. Study on adsorption of ammonia nitrogen by iron-loaded activated carbon from low temperature wastewater. *Chemosphere* **262**: 127895. https://doi.org/10.1016/j.chemosphere.2020.127895

Rezma S, Assaker IB, Chtourou R, Hafiane A, Deleuze H. 2019. Microporous activated carbon electrode derived from date stone without use of binder for capacitive deionization application. *Materials Research Bulletin* **111**: 222-229. https://doi.org/10.1016/j.materresbull.2018.11.030

Rozada F, Otero M, Moran A, Garcia A. 2005. Activated carbons from sewage sludge and discarded tyres: production and optimization. *Journal of hazardous materials* **124**: 181-191. https://doi.org/10.1016/j.jhazmat.2005.05.002

Sadhukhan B, Mondal NK, Chattoraj S. 2016. Optimisation using central composite design (CCD) and the desirability function for sorption of methylene blue from aqueous solution onto Lemna major. *Karbala International Journal of Modern Science* **2**: 145-155. https://doi.org/10.1016/j.kijoms.2016.03.005

Schneider DF. 2020. Machine learning and artificial intelligence. in Health Services Research, pp. 155-168. Springer. https://doi.org/10.1007/978-3-030-28357-5_14

Selmi T, Seffen M, Sammouda H, Mathieu S, Jagiello J, Celzard A, Fierro V. 2018. Physical meaning of the parameters used in fractal kinetic and generalised adsorption models of Brouers–Sotolongo. *Adsorption* **24**: 11-27. https://doi.org/10.1007/s10450-017-9927-9

Shahbazi D, Mousavi S, Nayeri D. 2020. Low-cost activated carbon: characterization, decolorization, modeling, optimization and kinetics. *International Journal of Environmental Science and Technology* **17**: 3935-3946. https://doi.org/10.1007/s13762-020-02698-w

Shahrokhi-Shahraki R, Benally C, El-Din MG, Park J. 2021. High efficiency removal of heavy metals using tire-derived activated carbon vs commercial activated carbon: Insights into the adsorption mechanisms. *Chemosphere* **264**: 128455. https://doi.org/10.1016/j.chemosphere.2020.128455

Shamsuddin M, Yusoff N, Sulaiman M. 2016. Synthesis and characterization of activated carbon produced from kenaf core fiber using H_3PO_4 activation. *Procedia Chemistry* **19**: 558-565. https://doi.org/10.1016/j.proche.2016.03.053

Singh B, Kumar P. 2020. Pre-treatment of petroleum refinery wastewater by coagulation and flocculation using mixed coagulant: Optimization of process parameters using response surface methodology (RSM). *Journal of Water Process Engineering* **36**: 101317. https://doi.org/10.1016/j.jwpe.2020.101317

Su M, Li H, He X, Xu Z. 2022. Significant enhancement of pesticide and organic dyes degradation by ion-exchange within a metal–organic framework. *Polyhedron* **215**: 115651. https://doi.org/10.1016/j.poly.2022.115651

Tahraoui H, Amrane A, Belhadj A-E, Zhang J. 2022a. Modeling the organic matter of water using the decision tree coupled with bootstrap aggregated and least-squares boosting. *Environmental Technology & Innovation* **27**: 102419. https://doi.org/10.1016/j.eti.2022.102419

Tahraoui H, Belhadj A-E, Amrane A, Houssein EH. 2022b. Predicting the concentration of sulfate using machine learning methods. *Earth Science Informatics*: 1-22. https://doi.org/10.1007/s12145-022-00785-9

Tahraoui H, Belhadj A-E, Hamitouche A-E. 2020. Prediction of the bicarbonate amount in drinking water in the region of Médéa using artificial neural network modelling. *Kemija u industriji: Časopis kemičara i kemijskih inženjera Hrvatske* **69**: 595-602. https://doi.org/10.15255/KUI.2020.002

Tahraoui H, Belhadj A-E, Hamitouche A-E, Bouhedda M, Amrane A. 2021a. Predicting the concentration of sulfate (So_4^{2-}) in drinking water using artificial neural networks: A case study: Médéa-algeria. *Desalination and Water Treatment* **217**: 181-194. https://doi.org/10.5004/dwt.2021.26813

Tahraoui H, Belhadj A-E, Moula N, Bouranene S, Amrane A. 2021b. Optimisation and prediction of the coagulant dose for the elimination of organic micropollutants based on turbidity. *Kemija u industriji* **70**: 675-691. https://doi.org/10.15255/KUI.2021.001

Tahraoui H, Belhadj A-E, Triki Z, Boudella NR, Seder S, Amrane A, Zhang J, Moula N, Tifoura A, Ferhat R et al. 2022c. Mixed Coagulant-flocculant Optimization for Pharmaceutical Effluent Pretreatment Using Response Surface Methodology and Gaussian Process Regression. *Process Safety and Environmental Protection*. https://doi.org/10.1016/j.psep.2022.11.045

*Tan K, Hameed B. 2017. Insight into the adsorption kinetics models for the removal of contaminants from aqueous solutions. Journal of the Taiwan Institute of Chemical Engineers **74**: 25-48.* https://doi.org/10.1016/j.jtice.2017.01.024

Tang X, Ran G, Li J, Zhang Z, Xiang C. 2021. Extremely efficient and rapidly adsorb methylene blue using porous adsorbent prepared from waste paper: Kinetics and equilibrium studies. *Journal of hazardous materials* **402**: 123579. https://doi.org/10.1016/j.jhazmat.2020.123579

Tarbaoui M, Oumam M, El Amraoui B, Fourmentin S, Benzina M, Charrouf M, Bennamara A, Abourriche A. 2014. Elaboration, caractérisation et évaluation des performances d'un nouveau matériau adsorbant à base des éponges marines: application dans l'adsorption des composés organiques volatils (Elaboration, characterization and evaluation of the performance of a new adsorbent material based of marine sponges: application in adsorption of volatile organic compounds). *J Mater Environ Sci* **5**: 2163-2168.

Teng X, Li J, Wang Z, Wei Z, Chen C, Du K, Zhao C, Yang G, Li Y. 2020. Performance and mechanism of methylene blue degradation by an electrochemical process. *RSC advances* **10**: 24712-24720. https://doi.org/10.1039/d0ra03963b

Teong C, Setiabudi H, El-Arish N, Bahari M, Teh L. 2021. Vatica rassak wood waste-derived activated carbon for effective Pb (II) adsorption: Kinetic, isotherm and reusability studies. Materials Today: Proceedings **42**: 165-171. https://doi.org/10.1016/j.matpr.2020.11.270

Thangappan H, Valiya Parambathu A, Joseph S. 2016. Surface characterization and methylene blue adsorption studies on a mesoporous adsorbent from chemically modified Areca triandra palm shell. *Desalination and Water Treatment* **57**: 21118-21129. https://doi.org/10.1080/19443994.2015.1111818

Tran HN, You S-J, Hosseini-Bandegharaei A, Chao H-P. 2017. Mistakes and inconsistencies regarding adsorption of contaminants from aqueous solutions: a critical review. *Water research* **120**: 88-116. https://doi.org/10.1016/j.watres.2017.04.014

Üner O, Geçgel Ü, Bayrak Y. 2016. Adsorption of methylene blue by an efficient activated carbon prepared from Citrullus lanatus rind: kinetic, isotherm, thermodynamic, and mechanism analysis. *Water, Air, & Soil Pollution* **227**: 1-15. https://doi.org/10.1007/s11270-016-2949-1

Wang H, Li Z, Yahyaoui S, Hanafy H, Seliem MK, Bonilla-Petriciolet A, Dotto GL, Sellaoui L, Li Q. 2021. Effective adsorption of dyes on an activated carbon prepared from carboxymethyl cellulose: Experiments, characterization and advanced modelling. *Chemical Engineering Journal* **417**: 128116. https://doi.org/10.1016/j.cej.2020.128116

Weber TW, Chakravorti RK. 1974. Pore and solid diffusion models for fixed-bed adsorbers. *AIChE Journal* **20**: 228-238. https://doi.org/10.1002/aic.690200204

Williams CK. 2005. *Gaussian processes for machine learning*. MIT press.

Witek-Krowiak A, Chojnacka K, Podstawczyk D, Dawiec A, Pokomeda K. 2014. Application of response surface methodology and artificial neural network methods in modelling and optimization of biosorption process. *Bioresource technology* **160**: 150-160. https://doi.org/10.1016/j.biortech.2014.01.021

Wu Q, Li W, Liu S, Jin C. 2016. Hydrothermal synthesis of N-doped spherical carbon from carboxymethylcellulose for CO_2 capture. *Applied Surface Science* **369**: 101-107. https://doi.org/10.1016/j.apsusc.2016.02.022

Ye G, Zhou J, Huang R, Ke Y, Peng Y, Zhou Y, Weng Y, Ling C, Pan W. 2022. Magnetic sludge-based biochar derived from Fenton sludge as an efficient heterogeneous Fenton catalyst for degrading Methylene blue. *Journal of Environmental Chemical Engineering* **10**: 107242. https://doi.org/10.1016/j.jece.2022.107242

Yeganeh MM, Kaghazchi T, Soleimani M. 2006. Effect of raw materials on properties of activated carbons. *Chemical Engineering & Technology: Industrial Chemistry-Plant Equipment-Process Engineering-Biotechnology* **29**: 1247-1251. https://doi.org/10.1002/ceat.200500298

Zhong Y, Yang Q, Li X, Chen H, Li X, Chen R, Liu Y, Zeng G. 2016. Multiparameter optimization of bromate sorption on anion exchange resin by a two-step statistical strategy: Plackett–Burman and Box–Behnken experimental design. *Desalination and Water Treatment* **57**: 15524-15532. https://doi.org/10.1080/19443994.2015.1072061